

This excerpt from  
Theoretical Neuroscience  
Computational and Mathematical Modeling of Neural Systems  
Peter Dayan and L. F. Abbott  
© 2001 The MIT Press.

is provided in screen-viewable form for personal use only by members  
of MIT CogNet.

Unauthorized use or dissemination of this information is expressly  
forbidden.

If you have any questions about this material, please contact  
[cognetadmin@cognet.mit.edu](mailto:cognetadmin@cognet.mit.edu).

# 5 Model Neurons I: Neuroelectronics

## 5.1 Introduction

A great deal is known about the biophysical mechanisms responsible for generating neuronal activity, and this knowledge provides a basis for constructing neuron models. Such models range from highly detailed descriptions involving thousands of coupled differential equations to greatly simplified caricatures useful for studying large interconnected networks. In this chapter, we discuss the basic electrical properties of neurons and the mathematical models by which they are described. We present a simple but nevertheless useful model neuron, the integrate-and-fire model, in a basic version and with added membrane and synaptic conductances. We also discuss the Hodgkin-Huxley model, which describes the conductances responsible for generating action potentials. In chapter 6, we continue by presenting more complex models, in terms of their conductances and morphology. Circuits and networks of model neurons are discussed in chapter 7. This chapter makes use of basic concepts of electrical circuit theory, which are reviewed in the Mathematical Appendix.

## 5.2 Electrical Properties of Neurons

Like other cells, neurons are packed with a huge number and variety of ions and molecules. A cubic micron of cytoplasm might contain, for example,  $10^{10}$  water molecules,  $10^8$  ions,  $10^7$  small molecules such as amino acids and nucleotides, and  $10^5$  proteins. Many of these molecules carry charges, either positive or negative. Most of the time, there is an excess concentration of negative charge inside a neuron. Excess charges that are mobile, like ions, repel each other and build up on the inside surface of the cell membrane. Electrostatic forces attract an equal density of positive ions from the extracellular medium to the outside surface of the membrane.

The cell membrane is a lipid bilayer 3 to 4 nm thick that is essentially impermeable to most charged molecules. This insulating feature causes the cell membrane to act as a capacitor by separating the charges lying

*cell membrane*

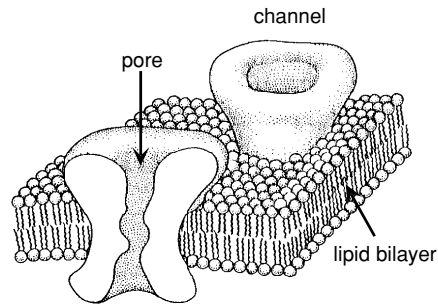


Figure 5.1 A schematic diagram of a section of the lipid bilayer that forms the cell membrane with two ion channels embedded in it. The membrane is 3 to 4 nm thick and the ion channels are about 10 nm long. (Adapted from Hille, 1992.)

#### *ion channels*

along its interior and exterior surfaces. Numerous ion-conducting channels embedded in the cell membrane (figure 5.1) lower the effective membrane resistance for ion flow to a value about 10,000 times smaller than that of a pure lipid bilayer. The resulting membrane conductance depends on the density and types of ion channels. A typical neuron may have a dozen or more different types of channels, anywhere from a few to hundreds of channels in a square micron of membrane, and hundreds of thousands to millions of channels in all. Many, but not all, channels are highly selective, allowing only a single type of ion to pass through them (to an accuracy of about 1 ion in  $10^4$ ). The capacity of channels for conducting ions across the cell membrane can be modified by many factors, including the membrane potential (voltage-dependent channels), the internal concentration of various intracellular messengers ( $\text{Ca}^{2+}$ -dependent channels, for example), and the extracellular concentration of neurotransmitters or neuromodulators (synaptic receptor channels, for example). The membrane also contains selective pumps that expend energy to maintain differences in the concentrations of ions inside and outside the cell.

#### *channel selectivity*

#### *ion pumps*

#### *membrane potential*

By convention, the potential of the extracellular fluid outside a neuron is defined to be 0. When a neuron is inactive, the excess internal negative charge causes the potential inside the cell membrane to be negative. This potential is an equilibrium point at which the flow of ions into the cell matches that out of the cell. The potential can change if the balance of ion flow is modified by the opening or closing of ion channels. Under normal conditions, neuronal membrane potentials vary over a range from about -90 to +50 mV. The order of magnitude of these potentials can be estimated from basic physical principles.

Membrane potentials are small enough to allow neurons to take advantage of thermal energy to help transport ions across the membrane, but are large enough so that thermal fluctuations do not swamp the signaling capabilities of the neuron. These conditions imply that potential differences across the cell membrane must lie in a range such that the energy gained or lost by an ion traversing the membrane is the same order of magnitude as its thermal energy. The thermal energy of an ion is about  $k_B T$  where  $k_B$

is the Boltzmann constant and  $T$  is the temperature on an absolute Kelvin scale. For chemists and biologists (though not for physicists), it is more customary to discuss moles of ions rather than single ions. A mole of ions has Avogadro's number times as much thermal energy as a single ion, or  $RT$ , where  $R$  is the universal gas constant, equal to  $8.31 \text{ joules/mol K}^\circ = 1.99 \text{ cal/mol K}^\circ$ .  $RT$  is about  $2500 \text{ joules/mol}$  or  $0.6 \text{ kCal/mol}$  at normal temperatures.

To estimate the size of typical membrane potentials, we equate the thermal energy of a mole of ions to the energy gained or lost when a mole of ions crosses a membrane with a potential difference  $V_T$  across it. This energy is  $FV_T$ , where  $F$  is the Faraday constant,  $F = 96,480 \text{ coulombs/mol}$ , equal to Avogadro's number times the charge of a single proton,  $q$ . Setting  $FV_T = RT$  gives

$$V_T = \frac{RT}{F} = \frac{k_B T}{q}. \quad (5.1)$$

This is an important parameter that enters into a number of calculations.  $V_T$  is between  $24$  and  $27 \text{ mV}$  for the typical temperatures of cold- and warm-blooded animals. This sets the overall scale for membrane potentials across neuronal membranes, which range from about  $-3$  to  $+2$  times  $V_T$ .

## Intracellular Resistance

Membrane potentials measured at different places within a neuron can take different values. For example, the potentials in the soma, dendrite, and axon can all be different. Potential differences between different parts of a neuron cause ions to flow within the cell, which tends to equalize these differences. The intracellular medium provides a resistance to such flow. This resistance is highest for long, narrow stretches of dendritic or axonal cable, such as the segment shown in figure 5.2. The longitudinal current  $I_L$  flowing along such a cable segment can be computed from Ohm's law. For the cylindrical segment of dendrite shown in figure 5.2, the longitudinal current flowing from right to left satisfies  $V_2 - V_1 = I_L R_L$ . Here,  $R_L$  is the longitudinal resistance, which grows in proportion to the length of the segment (long segments have higher resistances than short ones) and is inversely proportional to the cross-sectional area of the segment (thin segments have higher resistances than fat ones). The constant of proportionality, called the intracellular resistivity,  $r_L$ , typically falls in a range from  $1$  to  $3 \text{ k}\Omega \text{ mm}$ . The longitudinal resistance of the segment in figure 5.2 is  $r_L$  times the length  $L$  divided by the cross-sectional area  $\pi a^2$ ,  $R_L = r_L L / \pi a^2$ . A segment  $100 \mu\text{m}$  long with a radius of  $2 \mu\text{m}$  has a longitudinal resistance of about  $8 \text{ M}\Omega$ . A voltage difference of  $8 \text{ mV}$  would be required to force  $1 \text{ nA}$  of current down such a segment.

We can also use the intracellular resistivity to estimate crudely the conductance of a single channel. The conductance, being the inverse of a resistance, is equal to the cross-sectional area of the channel pore divided by

$V_T$

longitudinal  
current  $I_L$

longitudinal  
resistance  $R_L$

intracellular  
resistivity  $r_L$

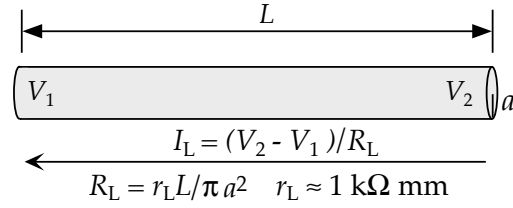


Figure 5.2 The longitudinal resistance of a cylindrical segment of neuronal cable with length  $L$  and radius  $a$ . The difference between the membrane potentials at the ends of this segment is related to the longitudinal current within the segment by Ohm's law, with  $R_L$  the longitudinal resistance of the segment. The arrow indicates the direction of positive current flow. The constant  $r_L$  is the intracellular resistivity, and a typical value is given.

single-channel  
conductance

its length and by  $r_L$ . We approximate the channel pore as a tube of length 6 nm and opening area  $0.15 \text{ nm}^2$ . This gives an estimate of  $0.15 \text{ nm}^2 / (1 \text{ k}\Omega \text{ mm} \times 6 \text{ nm}) \approx 25 \text{ pS}$ , which is the right order of magnitude for a channel conductance.

## Membrane Capacitance and Resistance

electrotonic  
compactness

The intracellular resistance to current flow can cause substantial differences in the membrane potential measured in different parts of a neuron, especially during rapid transient excursions of the membrane potential from its resting value, such as action potentials. Neurons that have few of the long, narrow cable segments that produce high longitudinal resistances may have relatively uniform membrane potentials across their surfaces. Such neurons are termed electrotonically compact. For electrotonically compact neurons, or for less compact neurons in situations where spatial variations in the membrane potential are not thought to play an important functional role, the entire neuron may be adequately described by a single membrane potential. Here, we discuss the membrane capacitance and resistance using such a description. An analysis for the case of spatially varying membrane potentials is presented in chapter 6.

membrane  
capacitance  $C_m$

specific membrane  
capacitance  $c_m$

We have mentioned that there is typically an excess negative charge on the inside surface of the cell membrane of a neuron, and a balancing positive charge on its outside surface (figure 5.3). In this arrangement, the cell membrane creates a capacitance  $C_m$ , and the voltage across the membrane  $V$  and the amount of this excess charge  $Q$  are related by the standard equation for a capacitor,  $Q = C_m V$ . The membrane capacitance is proportional to the total amount of membrane or, equivalently, to the surface area of the cell. The constant of proportionality, called the specific membrane capacitance, is the capacitance per unit area of membrane, and it is approximately the same for all neurons,  $c_m \approx 10 \text{ nF/mm}^2$ . The total capacitance  $C_m$  is the membrane surface area  $A$  times the specific capacitance,  $C_m = c_m A$ . Neuronal surface areas tend to be in the range  $0.01$  to  $0.1 \text{ mm}^2$ , so the membrane capacitance for a whole neuron is typically  $0.1$

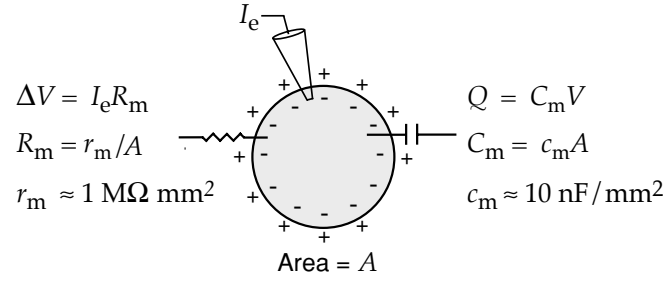


Figure 5.3 The capacitance and membrane resistance of a neuron considered as a single compartment. The membrane capacitance determines how the membrane potential  $V$  and excess internal charge  $Q$  are related. The membrane resistance  $R_m$  determines the size of the membrane potential deviation  $\Delta V$  caused by a small current  $I_e$  entering through an electrode, for example. Equations relating the total membrane capacitance and resistance,  $C_m$  and  $R_m$ , to the specific membrane capacitance and resistance,  $c_m$  and  $r_m$ , are given along with typical values of  $c_m$  and  $r_m$ . The value of  $r_m$  may vary considerably under different conditions and for different neurons.

to 1 nF. For a neuron with a total membrane capacitance of 1 nF,  $7 \times 10^{-11}$  coulomb or about  $10^9$  singly charged ions are required to produce a resting potential of -70 mV. This is about 1/100,000 of the total number of ions in a neuron and is the amount of charge delivered by a 0.7 nA current in 100 ms.

We can use the membrane capacitance to determine how much current is required to change the membrane potential at a given rate. The time derivative of the basic equation relating the membrane potential and charge,

$$C_m \frac{dV}{dt} = \frac{dQ}{dt}, \quad (5.2)$$

plays an important role in the mathematical modeling of neurons. The time derivative of the charge  $dQ/dt$  is equal to the current passing into the cell, so the amount of current needed to change the membrane potential of a neuron with a total capacitance  $C_m$  at a rate  $dV/dt$  is  $C_m dV/dt$ . For example, 1 nA will change the membrane potential of a neuron with a capacitance of 1 nF at a rate of 1 mV/ms.

The capacitance of a neuron determines how much current is required to make the membrane potential change at a given rate. Holding the membrane potential steady at a level different from its resting value also requires current, but this current is determined by the membrane resistance rather than by the capacitance of the cell. For example, if a small constant current  $I_e$  is injected into a neuron through an electrode, as in figure 5.3, the membrane potential will shift away from its resting value by an amount  $\Delta V$  given by Ohm's law,  $\Delta V = I_e R_m$ .  $R_m$  is known as the membrane or input resistance. The restriction to small currents and small  $\Delta V$  is required because membrane resistances can vary as a function of voltage, whereas Ohm's law assumes  $R_m$  is constant over the range  $\Delta V$ .

*membrane  
resistance  $R_m$*

membrane  
conductance

specific membrane  
resistance  $r_m$

The membrane resistance is the inverse of the membrane conductance, and, like the capacitance, the conductance of a piece of cell membrane is proportional to its surface area. The constant of proportionality is the membrane conductance per unit area, but we write it as  $1/r_m$ , where  $r_m$  is called the specific membrane resistance. Conversely, the membrane resistance  $R_m$  is equal to  $r_m$  divided by the surface area. When a neuron is in a resting state, the specific membrane resistance is around  $1 \text{ M}\Omega \text{ mm}^2$ . This number is much more variable than the specific membrane capacitance. Membrane resistances vary considerably among cells, and under different conditions and at different times for a given neuron, depending on the number, type, and state of its ion channels. For total surface areas between  $0.01$  and  $0.1 \text{ mm}^2$  the membrane resistance is typically in the range  $10$  to  $100 \text{ M}\Omega$ . With a  $100 \text{ M}\Omega$  membrane resistance, a constant current of  $0.1 \text{ nA}$  is required to hold the membrane potential  $10 \text{ mV}$  away from its resting value.

membrane time  
constant  $\tau_m$

The product of the membrane capacitance and the membrane resistance is a quantity with the units of time called the membrane time constant,  $\tau_m = R_m C_m$ . Because  $C_m$  and  $R_m$  have inverse dependences on the membrane surface area, the membrane time constant is independent of area and equal to the product of the specific membrane capacitance and resistance,  $\tau_m = r_m c_m$ . The membrane time constant sets the basic time scale for changes in the membrane potential and typically falls in the range between  $10$  and  $100 \text{ ms}$ .

## Equilibrium and Reversal Potentials

Electric forces and diffusion are responsible for driving ions through channel pores. Voltage differences between the exterior and interior of the cell produce forces on ions. Negative membrane potentials attract positive ions into the neuron and repel negative ions. In addition, ions diffuse through channels because the ion concentrations differ inside and outside the neuron. These differences are maintained by the ion pumps within the cell membrane. The concentrations of  $\text{Na}^+$  and  $\text{Ca}^{2+}$  are higher outside the cell than inside, so these ions are driven into the neuron by diffusion.  $\text{K}^+$  is more concentrated inside the neuron than outside, so it tends to diffuse out of the cell.

equilibrium  
potential

It is convenient to characterize the current flow due to diffusion in terms of an equilibrium potential. This is defined as the membrane potential at which current flow due to electric forces cancels the diffusive flow. For channels that conduct a single type of ion, the equilibrium potential can be computed easily. The potential difference across the cell membrane biases the flow of ions into or out of a neuron. Consider, for example, a positively charged ion and a negative membrane potential. In this case, the membrane potential opposes the flow of ions out of the cell. Ions can cross the membrane and leave the interior of the cell only if their thermal energy suffices to overcome the energy barrier produced by the membrane poten-

tial. If the ion has an electric charge  $zq$ , where  $q$  is the charge of one proton, it must have a thermal energy of at least  $-zqV$  to cross the membrane (this is a positive energy for  $z > 0$  and  $V < 0$ ). The probability that an ion has a thermal energy greater than or equal to  $-zqV$ , when the temperature (on an absolute scale) is  $T$ , is  $\exp(zqV/k_B T)$ . This is determined by integrating the Boltzmann distribution for energies greater than or equal to  $-zqV$ . In molar units, this result can be written as  $\exp(zFV/RT)$ , which is equal to  $\exp(zV/V_T)$  by equation 5.1.

The biasing effect of the electrical potential can be overcome by an opposing concentration gradient. A concentration of ions inside the cell, [inside], that is sufficiently greater than the concentration outside the cell, [outside], can compensate for the Boltzmann probability factor. The rate at which ions flow into the cell is proportional to [outside]. The flow of ions out of the cell is proportional to [inside] times the Boltzmann factor, because in this direction only those ions that have sufficient thermal energy can leave the cell. The net flow of ions will be 0 when the inward and outward flows are equal. We use the letter  $E$  to denote the particular potential that satisfies this balancing condition, which is then

$$[\text{outside}] = [\text{inside}] \exp(zE/V_T). \quad (5.3)$$

Solving this equation for  $E$ , we find

*Nernst equation*

$$E = \frac{V_T}{z} \ln \left( \frac{[\text{outside}]}{[\text{inside}]} \right). \quad (5.4)$$

Equation 5.4 is the Nernst equation. The reader can check that if the result is derived for either sign of ionic charge or membrane potential, the result is identical to 5.4, which thus applies in all cases. The equilibrium potential for a  $K^+$  conducting channel, labeled  $E_K$ , typically falls in the range between -70 and -90 mV. The  $Na^+$  equilibrium potential,  $E_{Na}$ , is 50 mV or higher, and  $E_{Ca}$ , for  $Ca^{2+}$  channels, is higher still, around 150 mV. Finally,  $Cl^-$  equilibrium potentials are typically around -60 to -65 mV, near the resting potential of many neurons.

The Nernst equation (5.4) applies when the channels that generate a particular conductance allow only one type of ion to pass through them. Some channels are not so selective, and in this case the potential  $E$  is not determined by equation 5.4. Instead, it takes a value intermediate between the equilibrium potentials of the individual ion types that it conducts. An approximate formula, known as the Goldman equation (see Tuckwell, 1988; or Johnston and Wu, 1995), can be used to estimate  $E$  for such conductances. In this case,  $E$  is often called a reversal potential, rather than an equilibrium potential, because the direction of current flow through the channel switches as the membrane potential passes through  $E$ .

*Goldman equation  
reversal potential*

A conductance with an equilibrium or reversal potential  $E$  tends to move the membrane potential of the neuron toward the value  $E$ . When  $V > E$ , this means that positive current will flow outward, and when  $V < E$ , positive current will flow inward. Because  $Na^+$  and  $Ca^{2+}$  conductances have



<i>depolarization</i>	positive reversal potentials, they tend to depolarize a neuron (make its membrane potential less negative). $K^+$ conductances, with their negative $E$ values, normally hyperpolarize a neuron (make its membrane potential more negative). $Cl^-$ conductances, with reversal potentials near the resting potential, may pass little net current. Instead, their primary impact is to change the membrane resistance of the cell. Such conductances are sometimes called shunting, although all conductances “shunt”, that is, increase the total conductance of a neuron. Synaptic conductances are also characterized by reversal potentials and are termed excitatory or inhibitory on this basis. Synapses with reversal potentials less than the threshold for action potential generation are typically called inhibitory, and those with reversal potentials above the action potential threshold are called excitatory.
<i>hyperpolarization</i>	
<i>shunting conductances</i>	
<i>inhibitory and excitatory synapses</i>	

## The Membrane Current

<i>membrane current per unit area <math>i_m</math></i>	The total current flowing across the membrane through all of its ion channels is called the membrane current of the neuron. By convention, the membrane current is defined as positive when positive ions leave the neuron and negative when positive ions enter the neuron. The total membrane current is determined by summing currents due to all of the different types of channels within the cell membrane, including voltage-dependent and synaptic channels. To facilitate comparisons between neurons of different sizes, it is convenient to use the membrane current per unit area of cell membrane, which we call $i_m$ . The total membrane current is obtained from $i_m$ by multiplying it by $A$ , the total surface area of the cell.
--	--

<i>driving force</i>	We label the different types of channels in a cell membrane with an index $i$ . As discussed in the last section, the current carried by a set of channels of type $i$ with reversal potential $E_i$ , vanishes when the membrane potential satisfies $V = E_i$ . For many types of channels, the current increases or decreases approximately linearly when the membrane potential deviates from this value. The difference $V - E_i$ is called the driving force, and the membrane current per unit area due to the type $i$ channels is written as $g_i(V - E_i)$ . The factor $g_i$ is the conductance per unit area, or specific conductance, due to these channels. Summing over the different types of channels, we obtain the total membrane current,
<i>specific conductance <math>g_i</math></i>	
<i>membrane current</i>	

$$i_m = \sum_i g_i(V - E_i). \quad (5.5)$$

Sometimes a more complicated expression called the Goldman-Hodgkin-Katz formula is used to relate the membrane current to  $g_i$  and membrane potential (see Tuckwell, 1988; or Johnston and Wu, 1995), but we will restrict our discussion to the simpler relationship used in equation 5.5.

Much of the complexity and richness of neuronal dynamics arises because membrane conductances change over time. However, some of the factors that contribute to the total membrane current can be treated as relatively constant, and these are typically grouped together into a single term

called the leakage current. The currents carried by ion pumps that maintain the concentration gradients that make equilibrium potentials nonzero typically fall into this category. For example, one type of pump uses the energy of ATP hydrolysis to move three  $\text{Na}^+$  ions out of the cell for every two  $\text{K}^+$  ions it moves in.

*leakage current*

It is normally assumed that ion pumps work at relatively steady rates so that the currents they generate can be included in a time-independent leakage conductance. Sometimes, this assumption is dropped and explicit pump currents are modeled. In either case, all of the time-independent contributions to the membrane current can be lumped together into a single leakage term  $\bar{g}_L(V - E_L)$ . Because this term hides many sins, its reversal potential  $E_L$  is not usually equal to the equilibrium potential of any specific ion. Instead, it is often kept as a free parameter and adjusted to make the resting potential of the model neuron match that of the cell being modeled. Similarly,  $\bar{g}_L$  is adjusted to match the membrane conductance at rest. The line over the parameter  $\bar{g}_L$  is used to indicate that it has constant value. A similar notation is used later in this chapter to distinguish variable conductances from the fixed parameters that describe them. The leakage conductance is called a passive conductance to distinguish it from variable conductances that are termed active.

*resting potential*

### 5.3 Single-Compartment Models

Models that describe the membrane potential of a neuron by a single variable  $V$  are called single-compartment models. This chapter deals exclusively with such models. Multi-compartment models, which can describe spatial variations in the membrane potential, are considered in chapter 6. The equations for single-compartment models, like those of all neuron models, describe how charges flow into and out of a neuron and affect its membrane potential.

Equation 5.2 provides the basic relationship that determines the membrane potential for a single-compartment model. This equation states that the rate of change of the membrane potential is proportional to the rate at which charge builds up inside the cell. The rate of charge buildup is, in turn, equal to the total amount of current entering the neuron. The relevant currents are those arising from all the membrane and synaptic conductances plus, in an experimental setting, any current injected into the cell through an electrode. From equation 5.2, the sum of these currents is equal to  $C_m dV/dt$ , the total capacitance of the neuron times the rate of change of the membrane potential. Because the membrane current is usually characterized as a current per unit area,  $i_m$ , it is more convenient to divide this relationship by the surface area of the neuron. Then, the total current per unit area is equal to  $c_m dV/dt$ , where  $c_m = C_m/A$  is the specific membrane capacitance. One complication in this procedure is that the electrode current,  $I_e$ , is not typically expressed as a current per unit area, so we must divide it by the total surface area of the neuron,  $A$ . Putting all

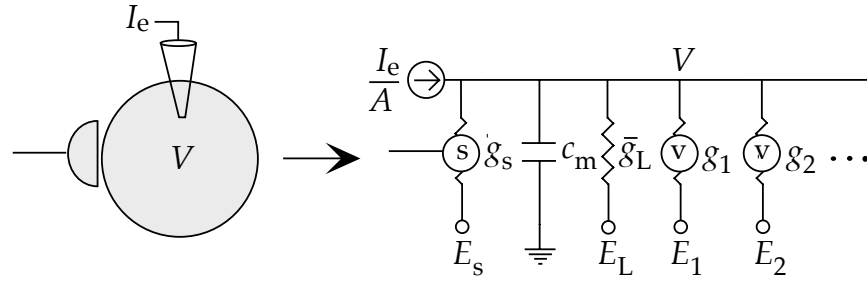


Figure 5.4 The equivalent circuit for a one-compartment neuron model. The neuron is represented, at the left, by a single compartment of surface area  $A$  with a synapse and a current-injecting electrode. At right is the equivalent circuit. The circled (s) indicates a synaptic conductance that depends on the activity of a presynaptic neuron. A single synaptic conductance  $g_s$  is indicated, but in general there may be several different types. The circled (v) indicates a voltage-dependent conductance, and  $I_e$  is the current passing through the electrode. The dots stand for possible additional membrane conductances.

this together, the basic equation for all single-compartment models is

$$c_m \frac{dV}{dt} = -i_m + \frac{I_e}{A}. \quad (5.6)$$

By convention, current that enters the neuron through an electrode is defined as positive-inward, whereas membrane current is defined as positive-outward. This explains the different signs for the currents in equation 5.6. The membrane current in equation 5.6 is determined by equation 5.5 and additional equations that specify the conductance variables  $g_i$ . The structure of such a model is the same as that of an electrical circuit, called the equivalent circuit, consisting of a capacitor and a set of variable and nonvariable resistors corresponding to the different membrane conductances. Figure 5.4 shows the equivalent circuit for a generic one-compartment model.

*equivalent circuit*

## 5.4 Integrate-and-Fire Models

A neuron will typically fire an action potential when its membrane potential reaches a threshold value of about -55 to -50 mV. During the action potential, the membrane potential follows a rapid, stereotyped trajectory and then returns to a value that is hyperpolarized relative to the threshold potential. As we will see, the mechanisms by which voltage-dependent  $K^+$  and  $Na^+$  conductances produce action potentials are well understood and can be modeled quite accurately. On the other hand, neuron models can be simplified and simulations can be accelerated dramatically if the biophysical mechanisms responsible for action potentials are not explicitly included in the model. Integrate-and-fire models do this by stipulating that an action potential occurs whenever the membrane potential of

the model neuron reaches a threshold value  $V_{\text{th}}$ . After the action potential, the potential is reset to a value  $V_{\text{reset}}$  below the threshold potential,  $V_{\text{reset}} < V_{\text{th}}$ .

The basic integrate-and-fire model was proposed by Lapicque in 1907, long before the mechanisms that generate action potentials were understood. Despite its age and simplicity, the integrate-and-fire model is still an extremely useful description of neuronal activity. By avoiding a biophysical description of the action potential, integrate-and-fire models are left with the simpler task of modeling only subthreshold membrane potential dynamics. This can be done with various levels of rigor. In the simplest version of these models, all active membrane conductances are ignored, including, for the moment, synaptic inputs, and the entire membrane conductance is modeled as a single passive leakage term,  $i_m = \bar{g}_L (V - E_L)$ . This version is called the passive or leaky integrate-and-fire model. For small fluctuations about the resting membrane potential, neuronal conductances are approximately constant, and the passive integrate-and-fire model assumes that this constancy holds over the entire subthreshold range. For some neurons this is a reasonable approximation, and for others it is not. With these approximations, the model neuron behaves like an electric circuit consisting of a resistor and a capacitor in parallel (figure 5.4), and the membrane potential is determined by equation 5.6 with  $i_m = \bar{g}_L (V - E_L)$ ,

*passive  
integrate-and-fire  
model*

$$c_m \frac{dV}{dt} = -\bar{g}_L (V - E_L) + \frac{I_e}{A}. \quad (5.7)$$

It is convenient to multiply equation 5.7 by the specific membrane resistance  $r_m$ , which in this case is given by  $r_m = 1/\bar{g}_L$ . This cancels the factor of  $\bar{g}_L$  on the right side of the equation and leaves a factor  $c_m r_m = \tau_m$  on the left side, where  $\tau_m$  is the membrane time constant of the neuron. The electrode current ends up being multiplied by  $r_m/A$ , which is the total membrane resistance  $R_m$ . Thus, the basic equation of the passive integrate-and-fire models is

$$\tau_m \frac{dV}{dt} = E_L - V + R_m I_e. \quad (5.8)$$

To generate action potentials in the model, equation 5.8 is augmented by the rule that whenever  $V$  reaches the threshold value  $V_{\text{th}}$ , an action potential is fired and the potential is reset to  $V_{\text{reset}}$ . Equation 5.8 indicates that when  $I_e = 0$ , the membrane potential relaxes exponentially with time constant  $\tau_m$  to  $V = E_L$ . Thus,  $E_L$  is the resting potential of the model cell.

The membrane potential for the passive integrate-and-fire model is determined by integrating equation 5.8 (a numerical method for doing this is described in appendix A) and applying the threshold and reset rule for action potential generation. The response of a passive integrate-and-fire model neuron to a time-varying electrode current is shown in figure 5.5.

The firing rate of an integrate-and-fire model in response to a constant injected current can be computed analytically. When  $I_e$  is independent of

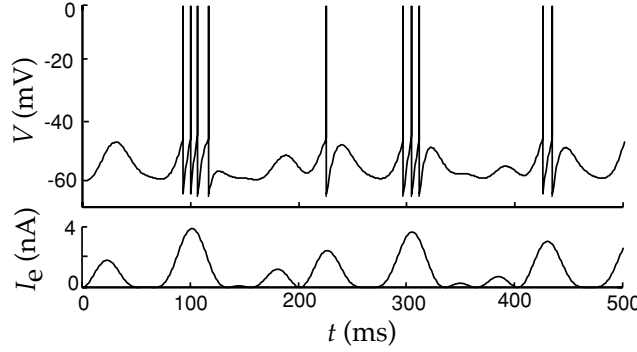


Figure 5.5 A passive integrate-and-fire model driven by a time-varying electrode current. The upper trace is the membrane potential, and the bottom trace the driving current. The action potentials in this figure are simply pasted onto the membrane potential trajectory whenever it reaches the threshold value. The parameters of the model are  $E_L = V_{\text{reset}} = -65$  mV,  $V_{\text{th}} = -50$  mV,  $\tau_m = 10$  ms, and  $R_m = 10$  M $\Omega$ .

time, the subthreshold potential  $V(t)$  can easily be computed by solving equation 5.8, and is

$$V(t) = E_L + R_m I_e + (V(0) - E_L - R_m I_e) \exp(-t/\tau_m), \quad (5.9)$$

where  $V(0)$  is the value of  $V$  at time  $t = 0$ . This solution can be checked by substituting it into equation 5.8. It is valid for the integrate-and-fire model only as long as  $V$  stays below the threshold. Suppose that at  $t = 0$ , the neuron has just fired an action potential and is thus at the reset potential, so that  $V(0) = V_{\text{reset}}$ . The next action potential will occur when the membrane potential reaches the threshold, that is, at a time  $t = t_{\text{isi}}$  when

$$V(t_{\text{isi}}) = V_{\text{th}} = E_L + R_m I_e + (V_{\text{reset}} - E_L - R_m I_e) \exp(-t_{\text{isi}}/\tau_m). \quad (5.10)$$

By solving this for  $t_{\text{isi}}$ , the time of the next action potential, we can determine the interspike interval for constant  $I_e$ , or equivalently its inverse, which we call the interspike-interval firing rate of the neuron,

$$r_{\text{isi}} = \frac{1}{t_{\text{isi}}} = \left( \tau_m \ln \left( \frac{R_m I_e + E_L - V_{\text{reset}}}{R_m I_e + E_L - V_{\text{th}}} \right) \right)^{-1}. \quad (5.11)$$

This expression is valid if  $R_m I_e > V_{\text{th}} - E_L$ ; otherwise  $r_{\text{isi}} = 0$ . For sufficiently large values of  $I_e$ , we can use the linear approximation of the logarithm ( $\ln(1+z) \approx z$  for small  $z$ ) to show that

$$r_{\text{isi}} \approx \left[ \frac{E_L - V_{\text{th}} + R_m I_e}{\tau_m (V_{\text{th}} - V_{\text{reset}})} \right]_+, \quad (5.12)$$

which shows that the firing rate grows linearly with  $I_e$  for large  $I_e$ .

Figure 5.6A compares  $r_{\text{isi}}$  as a function of  $I_e$ , using appropriate parameter values, with data from current injection into a cortical neuron in vivo. The firing rate of the cortical neuron in figure 5.6A has been defined as the

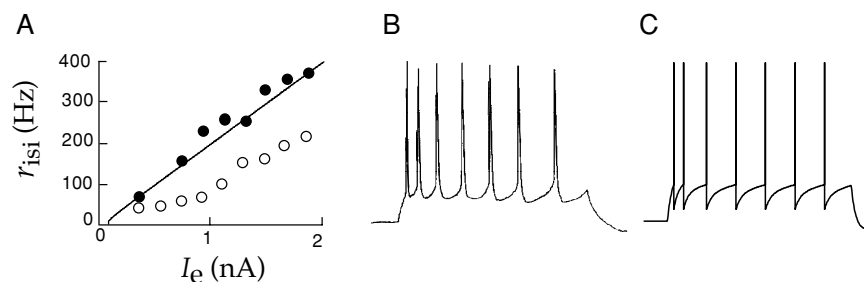


Figure 5.6 (A) Comparison of interspike-interval firing rates as a function of injected current for an integrate-and-fire model and a cortical neuron measure in vivo. The line gives  $r_{\text{isi}}$  for a model neuron with  $\tau_m = 30$  ms,  $E_L = V_{\text{reset}} = -65$  mV,  $V_{\text{th}} = -50$  mV, and  $R_m = 90$  M $\Omega$ . The data points are from a pyramidal cell in the primary visual cortex of a cat. The filled circles show the inverse of the interspike interval for the first two spikes fired, and the open circles show the steady-state interspike-interval firing rate after spike-rate adaptation. (B) A recording of the firing of a cortical neuron under constant current injection, showing spike-rate adaptation. (C) Membrane voltage trajectory and spikes for an integrate-and-fire model with an added current, with  $r_m \Delta g_{\text{sra}} = 0.06$ ,  $\tau_{\text{sra}} = 100$  ms, and  $E_K = -70$  mV (see equations 5.13 and 5.14). (Data in A from Ahmed et al., 1998; B from McCormick, 1990.)

inverse of the interval between pairs of spikes. The rates determined in this way, using the first two spikes fired by the neuron in response to the injected current (filled circles in figure 5.6A), agree fairly well with the results of the integrate-and-fire model described in the figure caption. However, the real neuron exhibits spike-rate adaptation, in that the interspike intervals lengthen over time when a constant current is injected into the cell (figure 5.6B), before settling to a steady-state value. The steady-state firing rate in figure 5.6A (open circles) could also be fitted by an integrate-and-fire model, but not using the same parameters that were used to fit the initial spikes. Spike-rate adaptation is a common feature of cortical pyramidal cells, and consideration of this phenomenon allows us to show how an integrate-and-fire model can be modified to incorporate more complex dynamics.

*spike-rate  
adaptation*

## Spike-Rate Adaptation and Refractoriness

The passive integrate-and-fire model that we have described thus far is based on two separate approximations, a highly simplified description of the action potential and a linear approximation for the total membrane current. If details of the action-potential generation process are not important for a particular modeling goal, the first approximation can be retained while the membrane current is modeled in as much detail as is necessary. We will illustrate this process by developing a heuristic description of spike-rate adaptation using a model conductance that has characteristics similar to measured neuronal conductances known to play important roles in producing this effect.

We model spike-rate adaptation by including an additional current in the model,

$$\tau_m \frac{dV}{dt} = E_L - V - r_m g_{\text{sra}} (V - E_K) + R_m I_e. \quad (5.13)$$

The spike-rate adaptation conductance  $g_{\text{sra}}$  has been modeled as a  $K^+$  conductance so, when activated, it will hyperpolarize the neuron, slowing any spiking that may be occurring. We assume that this conductance relaxes to 0 exponentially with time constant  $\tau_{\text{sra}}$  through the equation

$$\tau_{\text{sra}} \frac{dg_{\text{sra}}}{dt} = -g_{\text{sra}}. \quad (5.14)$$

Whenever the neuron fires a spike,  $g_{\text{sra}}$  is increased by an amount  $\Delta g_{\text{sra}}$ , that is,  $g_{\text{sra}} \rightarrow g_{\text{sra}} + \Delta g_{\text{sra}}$ . During repetitive firing, the current builds up in a sequence of steps causing the firing rate to adapt. Figures 5.6B and 5.6C compare the adapting firing pattern of a cortical neuron with the output of the model.

As discussed in chapter 1, the probability that a neuron fires is significantly reduced for a short period of time after the appearance of an action potential. Such a refractory effect is not included in the basic integrate-and-fire model. The simplest way of including an absolute refractory period in the model is to add a condition to the basic threshold crossing rule that forbids firing for a period of time immediately after a spike. Refractoriness can be incorporated in a more realistic way by adding a conductance similar to the spike-rate adaptation conductance discussed above, but with a faster recovery time and a larger conductance increment following an action potential. With a large increment, the current can essentially clamp the neuron to  $E_K$  following a spike, temporarily preventing further firing and producing an absolute refractory period. As this conductance relaxes back to 0, firing will be possible but initially less likely, producing a relative refractory period. When recovery is completed, normal firing can resume.

Another scheme that is sometimes used to model refractory effects is to raise the threshold for action-potential generation following a spike and then allow it to relax back to its normal value. Spike-rate adaptation can also be described by using an integrated version of the integrate-and-fire model known as the spike-response model, in which membrane potential waveforms are determined by summing precomputed postsynaptic potentials and after-spike hyperpolarizations. Finally, spike-rate adaptation and other effects can be incorporated into the integrate-and-fire framework by allowing the parameters  $\bar{g}_L$  and  $E_L$  in equation 5.7 to vary with time.

## 5.5 Voltage-Dependent Conductances

Most of the interesting electrical properties of neurons, including their ability to fire and propagate action potentials, arise from nonlinearities

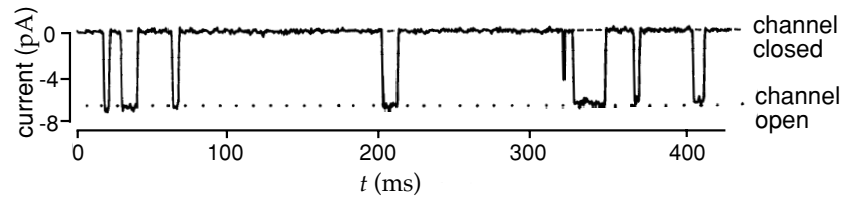


Figure 5.7 Recording of the current passing through a single ion channel. This is a synaptic receptor channel sensitive to the neurotransmitter acetylcholine. A small amount of acetylcholine was applied to the preparation to produce occasional channel openings. In the open state, the channel passes 6.6 pA at a holding potential of -140 mV. This is equivalent to more than  $10^7$  charges per second passing through the channel, and corresponds to an open channel conductance of 47 pS. (From Hille, 1992.)

associated with active membrane conductances. Recordings of the current flowing through single channels indicate that channels fluctuate rapidly between open and closed states in a stochastic manner (figure 5.7). Models of membrane and synaptic conductances must describe how the probability that a channel is in an open, ion-conducting state at any given time depends on the membrane potential (for a voltage-dependent conductance), the presence or absence of a neurotransmitter (for a synaptic conductance), or a number of other factors, such as the concentration of  $\text{Ca}^{2+}$  or other messenger molecules inside the cell. In this chapter, we consider two classes of active conductances, voltage-dependent membrane conductances and transmitter-dependent synaptic conductances. An additional type, the  $\text{Ca}^{2+}$ -dependent conductance, is considered in chapter 6.

*stochastic channel*

*voltage-dependent,  
synaptic, and  
 $\text{Ca}^{2+}$ -dependent  
conductances*

In a later section of this chapter, we discuss stochastic models of individual channels based on state diagrams and transition rates. However, most neuron models use deterministic descriptions of the conductances arising from many channels of a given type. This is justified because of the large number of channels of each type in the cell membrane of a typical neuron. If large numbers of channels are present, and if they fluctuate independently of each other (which they do, to a good approximation), then, from the law of large numbers, the fraction of channels open at any given time is approximately equal to the probability that any one channel is in an open state. This allows us to move between single-channel probabilistic formulations and macroscopic deterministic descriptions of membrane conductances.

We have denoted the conductance per unit area of membrane due to a set of ion channels of type  $i$  by  $g_i$ . The value of  $g_i$  at any given time is determined by multiplying the conductance of an open channel by the density of channels in the membrane and by the fraction of channels that are open at that time. The product of the first two factors is a constant called the maximal conductance that is denoted by  $\bar{g}_i$ . It is the conductance per unit area of membrane if all the channels of type  $i$  are open. Maximal conductance parameters tend to range from  $\mu\text{S}/\text{mm}^2$  to  $\text{mS}/\text{mm}^2$ . The fraction of channels in the open state is equivalent to the probability of finding any



*open probability  $P_i$*  given channel in the open state, and it is denoted by  $P_i$ . Thus,  $g_i = \bar{g}_i P_i$ . The dependence of a conductance on voltage, transmitter concentration, or other factors arises through effects on the open probability.

The open probability of a voltage-dependent conductance depends, as its name suggests, on the membrane potential of the neuron. In this chapter, we discuss models of two such conductances, the so-called delayed-rectifier  $K^+$  and fast  $Na^+$  conductances. The formalism we present, which is almost universally used to describe voltage-dependent conductances, was developed by Hodgkin and Huxley (1952) as part of their pioneering work showing how these conductances generate action potentials in the squid giant axon. Other conductances are modeled in chapter 6.

## Persistent Conductances

*channel gate*

*activation  
deactivation*

Figure 5.8 shows cartoons of the mechanisms by which voltage-dependent channels open and close as a function of membrane potential. Channels are depicted for two different types of conductances, termed persistent (figure 5.8A) and transient (figure 5.8B). We begin by discussing persistent conductances. Figure 5.8A shows a swinging gate attached to a voltage sensor that can open or close the pore of the channel. In reality, channel gating mechanisms involve complex changes in the conformational structure of the channel, but the simple swinging gate picture is sufficient if we are interested only in the current-carrying capacity of the channel. A channel that acts as if it had a single type of gate (although, as we will see, this is actually modeled as a number of identical subgates), like the channel in figure 5.8A, produces what is called a persistent or noninactivating conductance. Opening of the gate is called activation of the conductance, and gate closing is called deactivation. For this type of channel, the probability that the gate is open,  $P_K$ , increases when the neuron is depolarized and decreases when it is hyperpolarized. The delayed-rectifier  $K^+$  conductance that is responsible for repolarizing a neuron after an action potential is such a persistent conductance.

The opening of the gate that describes a persistent conductance may involve a number of conformational changes. For example, the delayed-rectifier  $K^+$  conductance is constructed from four identical subunits, and it appears that all four must undergo a structural change for the channel to open. In general, if  $k$  independent, identical events are required for a channel to open,  $P_K$  can be written as

$$P_K = n^k, \quad (5.15)$$

*activation  
variable  $n$*

where  $n$  is the probability that any one of the  $k$  independent gating events has occurred. Here,  $n$ , which varies between 0 and 1, is called a gating or an activation variable, and a description of its voltage and time dependence amounts to a description of the conductance. We can think of  $n$  as the probability of an individual subunit gate being open, and  $1 - n$  as the probability that it is closed.

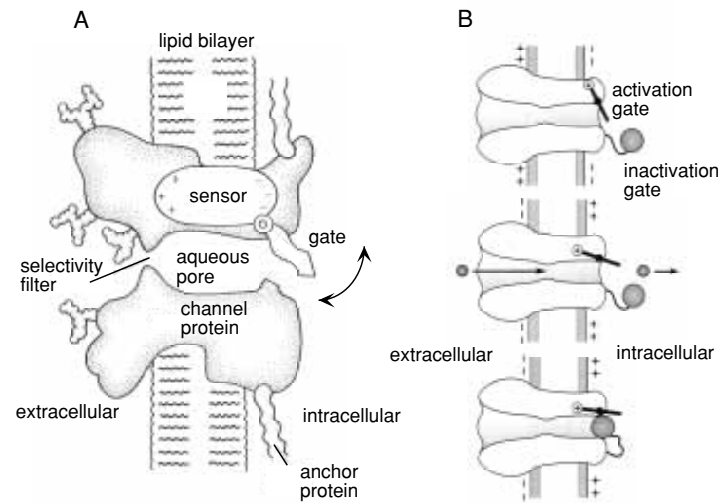


Figure 5.8 Gating of membrane channels. In both figures, the interior of the neuron is to the right of the membrane, and the extracellular medium is to the left. (A) A cartoon of gating of a persistent conductance. A gate is opened and closed by a sensor that responds to the membrane potential. The channel also has a region that selectively allows ions of a particular type to pass through the channel, for example,  $K^+$  ions for a potassium channel. (B) A cartoon of the gating of a transient conductance. The activation gate is coupled to a voltage sensor (denoted by a circled +) and acts like the gate in A. A second gate, denoted by the ball, can block that channel once it is open. The top figure shows the channel in a deactivated (and deactivated) state. The middle panel shows an activated channel, and the bottom panel shows an inactivated channel. Only the middle panel corresponds to an open, ion-conducting state. (A from Hille, 1992; B from Kandel et al., 1991.)

Although using the value of  $k = 4$  is consistent with the four-subunit structure of the delayed-rectifier conductance, in practice  $k$  is an integer chosen to fit the data, and should be interpreted as a functional definition of a subunit rather than a reflection of a realistic structural model of the channel. Indeed, the structure of the channel was not known at the time that Hodgkin and Huxley chose the form of equation 5.15 and suggested that  $k = 4$ .

We describe the transition of each subunit gate by a simple kinetic scheme in which the gating transition closed  $\rightarrow$  open occurs at a voltage-dependent rate  $\alpha_n(V)$ , and the reverse transition, open  $\rightarrow$  closed, occurs at a voltage-dependent rate  $\beta_n(V)$ . The probability that a subunit gate opens over a short interval of time is proportional to the probability of finding the gate closed,  $1 - n$ , multiplied by the opening rate  $\alpha_n(V)$ . Likewise, the probability that a subunit gate closes during a short time interval is proportional to the probability of finding the gate open,  $n$ , multiplied by the closing rate  $\beta_n(V)$ . The rate at which the open probability for a subunit gate changes is given by the difference of these two terms,

channel kinetics

opening rate  $\alpha_n(V)$

closing rate  $\beta_n(V)$

$$\frac{dn}{dt} = \alpha_n(V)(1 - n) - \beta_n(V)n. \quad (5.16)$$

The first term in equation 5.16 describes the opening process, and the second term the closing process (hence the minus sign) that lowers the probability of being in the configuration with an open subunit gate. Equation 5.16 can be written in another useful form by dividing through by  $\alpha_n(V) + \beta_n(V)$ ,

gating equation

$$\tau_n(V) \frac{dn}{dt} = n_\infty(V) - n, \quad (5.17)$$

$\tau_n(V)$  where

$$\tau_n(V) = \frac{1}{\alpha_n(V) + \beta_n(V)} \quad (5.18)$$

$n_\infty(V)$  and

$$n_\infty(V) = \frac{\alpha_n(V)}{\alpha_n(V) + \beta_n(V)}. \quad (5.19)$$

Equation 5.17 indicates that for a fixed voltage  $V$ ,  $n$  approaches the limiting value  $n_\infty(V)$  exponentially with time constant  $\tau_n(V)$ .

The key elements in the equation that determines  $n$  are the opening and closing rate functions  $\alpha_n(V)$  and  $\beta_n(V)$ . These are obtained by fitting experimental data. It is useful to discuss the form that we expect these rate functions to take on the basis of thermodynamic arguments. The state transitions described by  $\alpha_n$ , for example, are likely to be rate-limited by barriers requiring thermal energy. These transitions involve the movement of charged components of the gate across part of the membrane, so the height of these energy barriers should be affected by the membrane potential. The transition requires the movement of an effective charge, which we denote by  $qB_\alpha$ , through the potential  $V$ . This requires an energy  $qB_\alpha V$ . The constant  $B_\alpha$  reflects both the amount of charge being moved and the distance over which it travels. The probability that thermal fluctuations will provide enough energy to surmount this energy barrier is proportional to the Boltzmann factor,  $\exp(-qB_\alpha V/k_B T)$ . Based on this argument, we expect  $\alpha_n$  to be of the form

$$\alpha_n(V) = A_\alpha \exp(-qB_\alpha V/k_B T) = A_\alpha \exp(-B_\alpha V/V_T) \quad (5.20)$$

for some constant  $A_\alpha$ . The closing rate  $\beta_n$  should be expressed similarly, except with different constants  $A_\beta$  and  $B_\beta$ . From equation 5.19, we then find that  $n_\infty(V)$  is expected to be a sigmoidal function

$$n_\infty(V) = \frac{1}{1 + (A_\beta/A_\alpha) \exp((B_\alpha - B_\beta)V/V_T)}. \quad (5.21)$$

For a voltage-activated conductance, depolarization causes  $n$  to grow toward 1, and hyperpolarization causes  $n$  to shrink toward 0. Thus, we expect that the opening rate,  $\alpha_n$ , should be an increasing function of  $V$  (and thus  $B_\alpha < 0$ ), and  $\beta_n$  should be a decreasing function of  $V$  (and thus  $B_\beta > 0$ ). Examples of the functions we have discussed are plotted in figure 5.9.

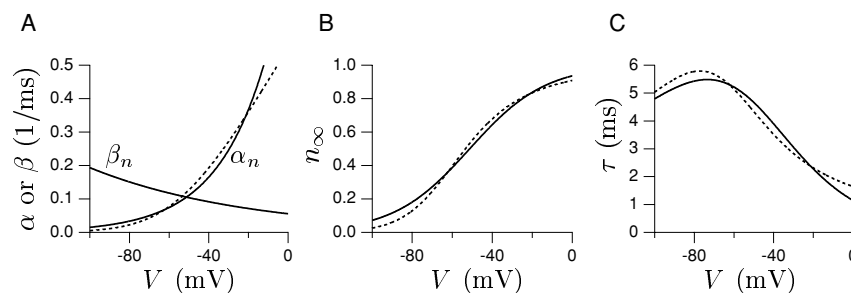


Figure 5.9 Generic voltage-dependent gating functions compared with Hodgkin-Huxley results for the delayed-rectifier  $K^+$  conductance. (A) The exponential  $\alpha_n$  and  $\beta_n$  functions expected from thermodynamic arguments are indicated by the solid curves. Parameter values used were  $A_\alpha = 1.22 \text{ ms}^{-1}$ ,  $A_\beta = 0.056 \text{ ms}^{-1}$ ,  $B_\alpha/V_T = -0.04/\text{mV}$ , and  $B_\beta/V_T = 0.0125/\text{mV}$ . The fit of Hodgkin and Huxley for  $\beta_n$  is identical to the solid curve shown. The Hodgkin-Huxley fit for  $\alpha_n$  is the dashed curve. (B) The corresponding function  $n_\infty(V)$  of equation 5.21 (solid curve). The dashed curve is obtained using the  $\alpha_n$  and  $\beta_n$  functions of the Hodgkin-Huxley fit (equation 5.22). (C) The corresponding function  $\tau_n(V)$ , obtained from equation 5.18 (solid curve). Again the dashed curve is the result of using the Hodgkin-Huxley rate functions.

While thermodynamic arguments support the forms we have presented, they rely on simplistic assumptions. Not surprisingly, the resulting functional forms do not always fit the data, and various alternatives are often employed. The data upon which these fits are based are typically obtained using a technique called voltage clamping. In this technique, an amplifier is configured to inject the appropriate amount of electrode current to hold the membrane potential at a constant value. By current conservation, this current is equal to the membrane current of the cell. Hodgkin and Huxley fitted the rate functions for the delayed-rectifier  $K^+$  conductance they studied, using the equations

$$\alpha_n = \frac{.01(V + 55)}{1 - \exp(-.1(V + 55))} \quad \text{and} \quad \beta_n = 0.125 \exp(-0.0125(V + 65)), \quad (5.22)$$

where  $V$  is expressed in mV, and  $\alpha_n$  and  $\beta_n$  are both expressed in units of  $1/\text{ms}$ . The fit for  $\beta_n$  is exactly the exponential form we have discussed, with  $A_\beta = 0.125 \exp(-0.0125 \cdot 65) \text{ ms}^{-1}$  and  $B_\beta/V_T = 0.0125 \text{ mV}^{-1}$ , but the fit for  $\alpha_n$  uses a different functional form. The dashed curves in figure 5.9 plot the formulas of equation 5.22.

## Transient Conductances

Some channels only open transiently when the membrane potential is depolarized because they are gated by two processes with opposite voltage dependences. Figure 5.8B is a schematic of a channel that is controlled by two gates and generates a transient conductance. The swinging gate in figure 5.8B behaves exactly like the gate in figure 5.8A. The probability that it

*voltage clamping*

activation  
variable  $m$

is open is written as  $m^k$ , where  $m$  is an activation variable similar to  $n$  and  $k$  is an integer. Hodgkin and Huxley used  $k = 3$  for their model of the fast  $\text{Na}^+$  conductance. The ball in figure 5.8B acts as the second gate. The probability that the ball does not block the channel pore is written as  $h$  and is called the inactivation variable. The activation and inactivation variables  $m$  and  $h$  are distinguished by having opposite voltage dependences. Depolarization causes  $m$  to increase and  $h$  to decrease, and hyperpolarization decreases  $m$  while increasing  $h$ .

inactivation  
variable  $h$

For the channel in figure 5.8B to conduct, both gates must be open, and assuming the two gates act independently, this has probability

$$P_{\text{Na}} = m^k h. \quad (5.23)$$

This is the general form used to describe the open probability for a transient conductance. We could raise the  $h$  factor in this expression to an arbitrary power, as we did for  $m$ , but we omit this complication to streamline the discussion. The activation  $m$  and inactivation  $h$ , like all gating variables, vary between 0 and 1. They are described by equations identical to 5.16, except that the rate functions  $\alpha_n$  and  $\beta_n$  are replaced by either  $\alpha_m$  and  $\beta_m$ , or  $\alpha_h$  and  $\beta_h$ . These rate functions were fitted by Hodgkin and Huxley using the equations (in units of  $1/\text{ms}$  with  $V$  in  $\text{mV}$ )

$$\begin{aligned} \alpha_m &= \frac{.1(V + 40)}{1 - \exp(-.1(V + 40))} & \beta_m &= 4 \exp(-.0556(V + 65)) \\ \alpha_h &= .07 \exp(-.05(V + 65)) & \beta_h &= 1/(1 + \exp(-.1(V + 35))). \end{aligned} \quad (5.24)$$

Functions  $m_\infty(V)$  and  $h_\infty(V)$  describing the steady-state activation and inactivation levels, and voltage-dependent time constants for  $m$  and  $h$  can be defined as in equations 5.19 and 5.18. These are plotted in figure 5.10. For comparison,  $n_\infty(V)$  and  $\tau_n(V)$  for the  $\text{K}^+$  conductance are also plotted. Note that  $h_\infty(V)$ , because it corresponds to an inactivation variable, is flipped relative to  $m_\infty(V)$  and  $n_\infty(V)$ , so that it approaches 1 at hyperpolarized voltages and 0 at depolarized voltages.

deinactivation

The presence of two factors in equation (5.23) gives a transient conductance some interesting properties. To turn on a transient conductance maximally, it may first be necessary to hyperpolarize the neuron below its resting potential and then to depolarize it. Hyperpolarization raises the value of the inactivation  $h$ , a process called deinactivation. The second step, depolarization, increases the value of  $m$ , which is activation. Only when  $m$  and  $h$  are both nonzero is the conductance turned on. Note that the conductance can be reduced in magnitude by either decreasing  $m$  or  $h$ . Decreasing  $h$  is called inactivation to distinguish it from decreasing  $m$ , which is deactivation.

inactivation

## Hyperpolarization-Activated Conductances

Persistent currents act as if they are controlled by an activation gate, while transient currents act as if they have both an activation and an inactivation

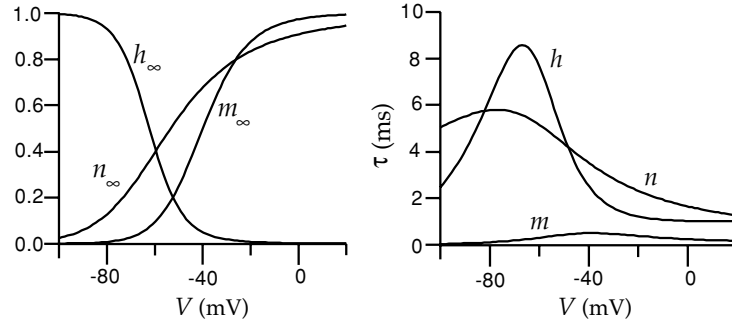


Figure 5.10 The voltage-dependent functions of the Hodgkin-Huxley model. The left panel shows  $m_\infty(V)$ ,  $h_\infty(V)$ , and  $n_\infty(V)$ , the steady-state levels of activation and inactivation of the  $\text{Na}^+$  conductance, and activation of the  $\text{K}^+$  conductance. The right panel shows the voltage-dependent time constants that control the rates at which these steady-state levels are approached for the three gating variables.

gate. Another class of conductances, the hyperpolarization-activated conductances, behave as if they are controlled solely by an inactivation gate. They are thus persistent conductances, but they open when the neuron is hyperpolarized rather than depolarized. The opening probability for such channels is written solely in terms of an inactivation variable similar to  $h$ . Strictly speaking, these conductances deinactivate when they turn on and inactivate when they turn off. However, most people cannot bring themselves to say “deinactivate” all the time, so they say instead that these conductances are activated by hyperpolarization.

## 5.6 The Hodgkin-Huxley Model

The Hodgkin-Huxley model for the generation of the action potential, in its single-compartment form, is constructed by writing the membrane current in equation 5.6 as the sum of a leakage current, a delayed-rectified  $\text{K}^+$  current, and a transient  $\text{Na}^+$  current,

$$i_m = \bar{g}_L(V - E_L) + \bar{g}_K n^4(V - E_K) + \bar{g}_{\text{Na}} m^3 h(V - E_{\text{Na}}). \quad (5.25)$$

The maximal conductances and reversal potentials used in the model are  $\bar{g}_L = 0.003 \text{ mS/mm}^2$ ,  $\bar{g}_K = 0.36 \text{ mS/mm}^2$ ,  $\bar{g}_{\text{Na}} = 1.2 \text{ mS/mm}^2$ ,  $E_L = -54.387 \text{ mV}$ ,  $E_K = -77 \text{ mV}$  and  $E_{\text{Na}} = 50 \text{ mV}$ . The full model consists of equation 5.6 with equation 5.25 for the membrane current, and equations of the form 5.17 for the gating variables  $n$ ,  $m$ , and  $h$ . These equations can be integrated numerically, using the methods described in appendices A and B.

The temporal evolution of the dynamic variables of the Hodgkin-Huxley model during a single action potential is shown in figure 5.11. The initial rise of the membrane potential, prior to the action potential, seen in the upper panel of figure 5.11, is due to the injection of a positive electrode current into the model starting at  $t = 5 \text{ ms}$ . When this current drives the

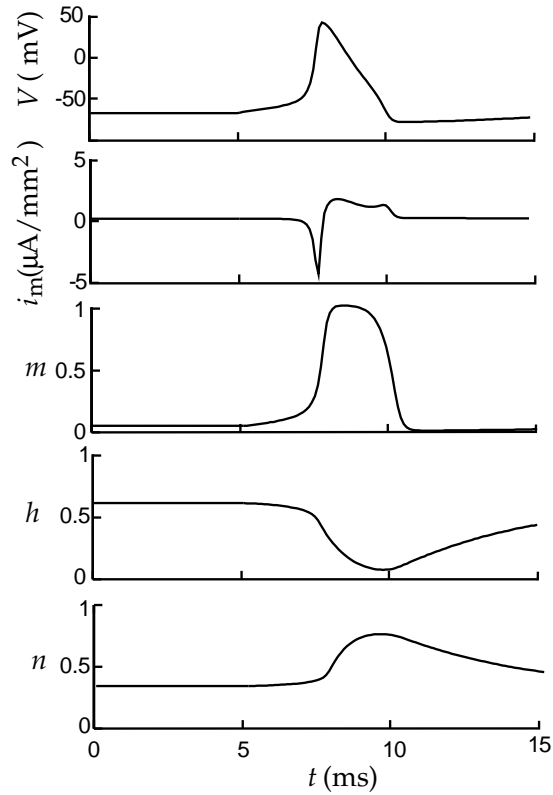


Figure 5.11 The dynamics of  $V$ ,  $m$ ,  $h$ , and  $n$  in the Hodgkin-Huxley model during the firing of an action potential. The upper-most trace is the membrane potential, the second trace is the membrane current produced by the sum of the Hodgkin-Huxley  $K^+$  and  $Na^+$  conductances, and subsequent traces show the temporal evolution of  $m$ ,  $h$ , and  $n$ . Current injection was initiated at  $t = 5$  ms.

membrane potential up to about -50 mV, the  $m$  variable that describes activation of the  $Na^+$  conductance suddenly jumps from nearly 0 to a value near 1. Initially, the  $h$  variable, expressing the degree of inactivation of the  $Na^+$  conductance, is around 0.6. Thus, for a brief period both  $m$  and  $h$  are significantly different from 0. This causes a large influx of  $Na^+$  ions, producing the sharp downward spike of inward current shown in the second trace from the top. The inward current pulse causes the membrane potential to rise rapidly to around 50 mV (near the  $Na^+$  equilibrium potential). The rapid increase in both  $V$  and  $m$  is due to a positive feedback effect. Depolarization of the membrane potential causes  $m$  to increase, and the resulting activation of the  $Na^+$  conductance makes  $V$  increase. The rise in the membrane potential causes the  $Na^+$  conductance to inactivate by driving  $h$  toward 0. This shuts off the  $Na^+$  current. In addition, the rise in  $V$  activates the  $K^+$  conductance by driving  $n$  toward 1. This increases the  $K^+$  current, which drives the membrane potential back down to negative values. The final recovery involves the readjustment of  $m$ ,  $h$ , and  $n$  to their initial values.

The Hodgkin-Huxley model can also be used to study propagation of an action potential down an axon, but for this purpose a multi-compartment model must be constructed. Methods for building such a model, and results from it, are described in chapter 6.

## 5.7 Modeling Channels

In previous sections, we described the Hodgkin-Huxley formalism for describing voltage-dependent conductances arising from a large number of channels. With the advent of single-channel studies, microscopic descriptions of the transitions between the conformational states of channel molecules have been developed. Because these models describe complex molecules, they typically involve many states and transitions. Here, we discuss simple versions of these models that capture the spirit of single-channel modeling without getting mired in the details.

Models of single channels are based on state diagrams that indicate the possible conformational states that the channel can assume. Typically, one of the states in the diagram is designated as open and ion-conducting, while the other states are nonconducting. The current conducted by the channel is written as  $\bar{g}P(V - E)$ , where  $E$  is the reversal potential,  $\bar{g}$  is the single-channel open conductance, and  $P$  is 1 whenever the open state is occupied, and 0 otherwise. Channel models can be instantiated directly from state diagrams simply by keeping track of the state of the channel and allowing stochastic changes of state to occur at appropriate transition rates. If the model is updated in short time steps of duration  $\Delta t$ , the probability that the channel makes a given transition during an update interval is the transition rate times  $\Delta t$ .

Figure 5.12 shows the state diagram and simulation results for a model of a single delayed-rectifier  $K^+$  channel that is closely related to the Hodgkin-Huxley description of the macroscopic delayed-rectifier conductance. The factors  $\alpha_n$  and  $\beta_n$  in the transition rates shown in the state diagram of figure 5.12 are the voltage-dependent rate functions of the Hodgkin-Huxley model. The model uses the same four subunit structure assumed in the Hodgkin-Huxley model. We can think of state 1 in this diagram as a state in which all the subunit gates are closed. States 2, 3, 4, and 5 have 1, 2, 3, and 4 open subunit gates, respectively. State 5 is the sole open state. The factors of 1, 2, 3, and 4 in the transition rates in figure 5.12 correspond to the number of subunit gates that can make a given transition. For example, the transition rate from state 1 to state 2 is four times faster than the rate from state 4 to state 5. This is because any one of the four subunit gates can open to get from state 1 to state 2, but the transition from state 4 to state 5 requires the single remaining closed subunit gate to open.

The lower panels in figure 5.12 show simulations of this model involving 1, 10, and 100 channels. The sum of currents from all of these channels is compared with the current predicted by the Hodgkin-Huxley model



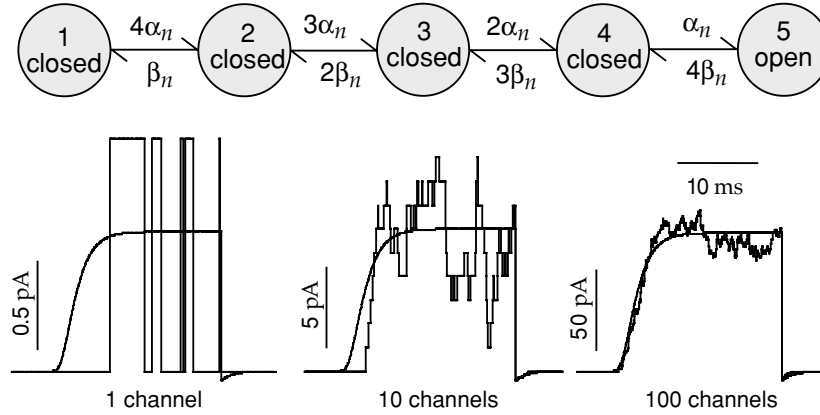


Figure 5.12 A model of the delayed-rectifier  $K^+$  channel. The upper diagram shows the states and transition rates of the model. In the simulations shown in the lower panels, the membrane potential was initially held at  $-100$  mV, then held at  $10$  mV for  $20$  ms, and finally returned to a holding potential of  $-100$  mV. The smooth curves in these panels show the membrane current predicted by the Hodgkin-Huxley model in this situation. The left panel shows a simulation of a single channel that opened several times during the depolarization. The middle panel shows the total current from  $10$  simulated channels, and the right panel corresponds to  $100$  channels. As the number of channels increases, the Hodgkin-Huxley model provides a more accurate description of the current.

(scaled by the appropriate maximal conductance). For each channel, the pattern of opening and closing is random, but when enough channels are summed, the total current matches that of the Hodgkin-Huxley model quite well.

To see how the channel model in figure 5.12 reproduces the results of the Hodgkin-Huxley model when the currents from many channels are summed, we must consider a probabilistic description of the channel model. We denote the probability that a channel is in state  $a$  of figure 5.12 by  $p_a$ , with  $a = 1, 2, \dots, 5$ . Dynamic equations for these probabilities are easily derived by setting the rate of change for a given  $p_a$  equal to the probability per unit time of entry into state  $a$  from other states minus the rate for leaving state  $a$ . The entry probability per unit time is the product of the appropriate transition rate times the probability that the state making the transition is occupied. The probability per unit time for leaving is  $p_a$  times the sum of all the rates for possible transitions out of the state. Following this reasoning, the equations for the state probabilities are (using the notation  $\dot{p} = dp/dt$ )

$$\begin{aligned}
 \dot{p}_1 &= \beta_n p_2 - 4\alpha_n p_1 \\
 \dot{p}_2 &= 4\alpha_n p_1 + 2\beta_n p_3 - (\beta_n + 3\alpha_n) p_2 \\
 \dot{p}_3 &= 3\alpha_n p_2 + 3\beta_n p_4 - (2\beta_n + 2\alpha_n) p_3 \\
 \dot{p}_4 &= 2\alpha_n p_3 + 4\beta_n p_5 - (3\beta_n + \alpha_n) p_4 \\
 \dot{p}_5 &= \alpha_n p_4 - 4\beta_n p_5.
 \end{aligned} \tag{5.26}$$

A solution for these equations can be constructed if we recall that, in the

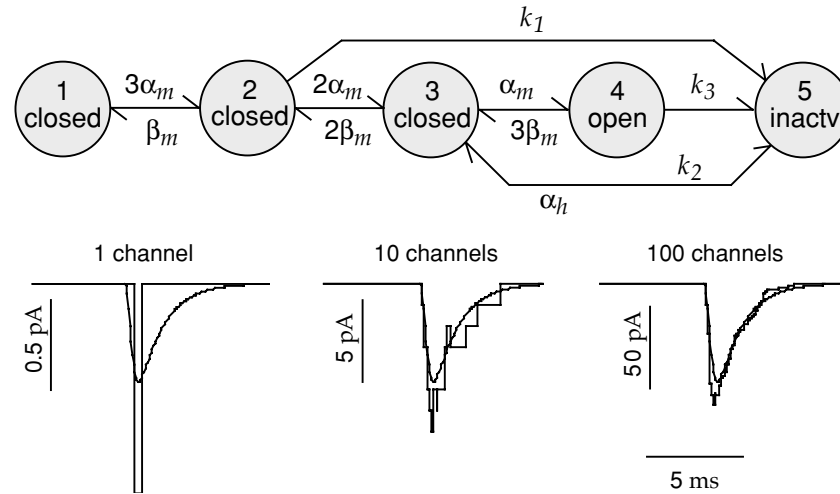


Figure 5.13 A model of the fast  $\text{Na}^+$  channel. The upper diagram shows the states and transitions rates of the model. The values  $k_1 = 0.24/\text{ms}$ ,  $k_2 = 0.4/\text{ms}$ , and  $k_3 = 1.5/\text{ms}$  were used in the simulations shown in the lower panels. For these simulations, the membrane potential was initially held at  $-100$  mV, then held at  $10$  mV for  $20$  ms, and finally returned to a holding potential of  $-100$  mV. The smooth curves in these panels show the current predicted by the Hodgkin-Huxley model in this situation. The left panel shows a simulation of a single channel that opened once during the depolarization. The middle panel shows the total current from  $10$  simulated channels, and the right panel corresponds to  $100$  channels. As the number of channels increases, the Hodgkin-Huxley model provides a fairly accurate description of the current, but it is not identical to the channel model in this case.

Hodgkin-Huxley model,  $n$  is the probability of a subunit gate being in the open state and  $1 - n$  is the probability of it being closed. If we use that same notation here, state 1 has four closed subunit gates, and thus  $p_1 = (1 - n)^4$ . State 5, the open state, has four open subunit gates, so  $p_5 = n^4 = P$ . State 2 has one open subunit gate, which can be any one of the four subunit gates, and three closed states, making  $p_2 = 4n(1 - n)^3$ . Similar arguments yield  $p_3 = 6n^2(1 - n)^2$  and  $p_4 = 4n^3(1 - n)$ . These expressions generate a solution to the above equations, provided that  $n$  satisfies equation 5.16, as the reader can verify.

In the Hodgkin-Huxley model of the  $\text{Na}^+$  conductance, the activation and inactivation processes are assumed to act independently. The schematic in figure 5.8B, which cartoons the mechanism believed to be responsible for inactivation, suggests that this assumption is incorrect. The ball that inactivates the channel is located inside the cell membrane, where it cannot be affected directly by the potential across the membrane. Furthermore, in this scheme the ball cannot occupy the channel pore until the activation gate has opened, making the two processes interdependent.

The state diagram in figure 5.13 reflects this by having a state-dependent, voltage-independent inactivation mechanism. This diagram is a simplified version of an  $\text{Na}^+$  channel model due to Patlak (1991). The sequence of transitions that lead to channel opening through states 1, 2, 3, and 4 is

*state-dependent  
inactivation*

identical to that of the Hodgkin-Huxley model, with transition rates determined by the Hodgkin-Huxley functions  $\alpha_m(V)$  and  $\beta_m(V)$  and appropriate combinatoric factors. State 4 is the open state. The transition to the inactivated state 5, however, is quite different from the inactivation process in the Hodgkin-Huxley model. Inactivation transitions to state 5 can occur only from states 2, 3, and 4, and the corresponding transition rates  $k_1$ ,  $k_2$ , and  $k_3$  are constants, independent of voltage. The deinactivation process occurs at the Hodgkin-Huxley rate  $\alpha_h(V)$  from state 5 to state 3.

Figure 5.13 shows simulations of this  $\text{Na}^+$  channel model. In contrast to the  $\text{K}^+$  channel model shown in figure 5.12, this model does not reproduce exactly the results of the Hodgkin-Huxley model when large numbers of channels are summed. Nevertheless, the two models agree quite well, as seen in the lower right panel of figure 5.13. The agreement, despite the different mechanisms of inactivation, is due to the speed of the activation process for the  $\text{Na}^+$  conductance. The inactivation rate function  $\beta_h(V)$  in the Hodgkin-Huxley model has a sigmoidal form similar to the asymptotic activation function  $m_\infty(V)$  (see equation 5.24). This is indicative of the actual dependence of inactivation on  $m$  and not on  $V$ . However, the activation variable  $m$  of the Hodgkin-Huxley model reaches its voltage-dependent asymptotic value  $m_\infty(V)$  so rapidly that it is difficult to distinguish inactivation processes that depend on  $m$  from those that depend on  $V$ . Differences between the two models are apparent only during a sub-millisecond time period while the conductance is activating. Experiments that can resolve this time scale support the channel model over the original Hodgkin-Huxley description.

## 5.8 Synaptic Conductances

Synaptic transmission at a spike-mediated chemical synapse begins when an action potential invades the presynaptic terminal and activates voltage-dependent  $\text{Ca}^{2+}$  channels, leading to a rise in the concentration of  $\text{Ca}^{2+}$  within the terminal. This causes vesicles containing transmitter molecules to fuse with the cell membrane and release their contents into the synaptic cleft between the pre- and postsynaptic sides of the synapse. The transmitter molecules then diffuse across the cleft and bind to receptors on the postsynaptic neuron. Binding of transmitter molecules leads to the opening of ion channels that modify the conductance of the postsynaptic neuron, completing the transmission of the signal from one neuron to the other. Postsynaptic ion channels can be activated directly by binding to the transmitter, or indirectly when the transmitter binds to a distinct receptor that affects ion channels through an intracellular second-messenger signaling pathway.

As with a voltage-dependent conductance, a synaptic conductance can be written as the product of a maximal conductance and an open channel probability,  $g_s = \bar{g}_s P$ . The open probability for a synaptic conductance can be expressed as a product of two terms that reflect processes occurring on

the pre- and postsynaptic sides of the synapse,  $P = P_s P_{\text{rel}}$ . The factor  $P_s$  is the probability that a postsynaptic channel opens, given that the transmitter was released by the presynaptic terminal. Because there are typically many postsynaptic channels, this can also be taken as the fraction of channels opened by the transmitter.

*synaptic open  
probability  $P_s$*

$P_{\text{rel}}$  is related to the probability that transmitter is released by the presynaptic terminal following the arrival of an action potential. This reflects the fact that transmitter release is a stochastic process. Release of transmitter at a presynaptic terminal does not necessarily occur every time an action potential arrives and, conversely, spontaneous release can occur even in the absence of the depolarization due to an action potential. The interpretation of  $P_{\text{rel}}$  is a bit subtle because a synaptic connection between neurons may involve multiple anatomical synapses, and each of these may have multiple independent transmitter release sites. The factor  $P_{\text{rel}}$ , in our discussion, is the average of the release probabilities at each release site. If there are many release sites, the total amount of transmitter released by all the sites is proportional to  $P_{\text{rel}}$ . If there is a single release site,  $P_{\text{rel}}$  is the probability that it releases transmitter. We will restrict our discussion to these two interpretations of  $P_{\text{rel}}$ . For a modest number of release sites with widely varying release probabilities, the current we discuss describes only an average over multiple trials.

*transmitter release  
probability  $P_{\text{rel}}$*

Synapses can exert their effects on the soma, dendrites, axon spike-initiation zone, or presynaptic terminals of their postsynaptic targets. There are two broad classes of synaptic conductances that are distinguished by whether the transmitter binds to the synaptic channel and activates it directly, or the transmitter binds to a distinct receptor that activates the conductance indirectly through an intracellular signaling pathway. The first class is called ionotropic and the second, metabotropic. Ionotropic conductances activate and deactivate more rapidly than metabotropic conductances. Metabotropic receptors can, in addition to opening channels, cause long-lasting changes inside a neuron. They typically operate through pathways that involve G-protein-mediated receptors and various intracellular signaling molecules known as second messengers. Many neuromodulators, including serotonin, dopamine, norepinephrine, and acetylcholine, act through metabotropic receptors. These have a wide variety of important effects on the functioning of the nervous system.

*ionotropic receptor*

*metabotropic  
receptor*

Glutamate and GABA ( $\gamma$ -aminobutyric acid) are the major excitatory and inhibitory transmitters in the brain. Both act ionotropically and metabotropically. The principal ionotropic receptor types for glutamate are called AMPA and NMDA. Both AMPA and NMDA receptors produce mixed-activation conductances with reversal potentials around 0 mV. The AMPA current activates and deactivates rapidly. The NMDA receptor is somewhat slower to activate and deactivates considerably more slowly. In addition, NMDA receptors have an unusual voltage dependence that we discuss in a later section, and are more permeable to  $\text{Ca}^{2+}$  than AMPA receptors.

*glutamate, GABA*

*AMPA, NMDA*

$GABA_A, GABA_B$	GABA activates two important inhibitory synaptic conductances in the brain. $GABA_A$ receptors produce a relatively fast ionotropic $Cl^-$ conductance. $GABA_B$ receptors are metabotropic, and act to produce a slower and longer-lasting $K^+$ conductance.
<i>gap junctions</i>	In addition to chemical synapses, neurons can be coupled through electrical synapses (gap junctions) that produce a synaptic current proportional to the difference between the pre- and postsynaptic membrane potentials. Some gap junctions rectify so that positive and negative current flows are not equal for potential differences of the same magnitude.

## The Postsynaptic Conductance

In a simple model of a directly activated receptor channel, the transmitter interacts with the channel through a binding reaction in which  $k$  transmitter molecules bind to a closed receptor and open it. In the reverse reaction, the transmitter molecules unbind from the receptor and it closes. These processes are analogous to the opening and closing involved in the gating of a voltage-dependent channel, and the same type of equation is used to describe how the open probability  $P_s$  changes with time,

$$\frac{dP_s}{dt} = \alpha_s(1 - P_s) - \beta_s P_s. \quad (5.27)$$

Here,  $\beta_s$  determines the closing rate of the channel and is usually assumed to be a constant. The opening rate,  $\alpha_s$ , on the other hand, depends on the concentration of transmitter available for binding to the receptor. If the concentration of transmitter at the site of the synaptic channel is  $[transmitter]$ , the probability of finding  $k$  transmitter molecules within binding range of the channel is proportional to  $[transmitter]^k$ , and  $\alpha_s$  is some constant of proportionality times this factor.

When an action potential invades the presynaptic terminal, the transmitter concentration rises and  $\alpha_s$  grows rapidly, causing  $P_s$  to increase. Following the release of transmitter, diffusion out of the cleft, enzyme-mediated degradation, and presynaptic uptake mechanisms can all contribute to a rapid reduction of the transmitter concentration. This sets  $\alpha_s$  to 0, and  $P_s$  follows suit by decaying exponentially with a time constant  $1/\beta_s$ . Typically, the time constant for channel closing is considerably larger than the opening time.

As a simple model of transmitter release, we assume that the transmitter concentration in the synaptic cleft rises extremely rapidly after vesicle release, remains at a high value for a period of duration  $T$ , and then falls rapidly to 0. Thus, the transmitter concentration is modeled as a square pulse. While the transmitter concentration is nonzero,  $\alpha_s$  takes a constant value much greater than  $\beta_s$ , otherwise  $\alpha_s = 0$ . Suppose that vesicle release occurs at time  $t = 0$  and that the synaptic channel open probability takes the value  $P_s(0)$  at this time. While the transmitter concentration in the cleft

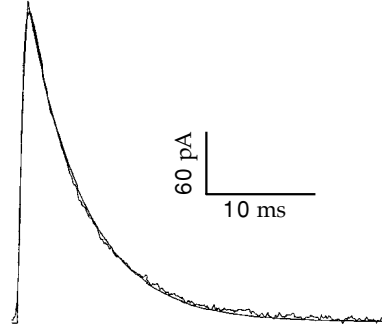


Figure 5.14 A fit of the model discussed in the text to the average EPSC (excitatory postsynaptic current) recorded from mossy fiber input to a CA3 pyramidal cell in a hippocampal slice preparation. The smooth line is the theoretical curve and the wiggly line is the result of averaging recordings from a number of trials. (Adapted from Destexhe et al., 1994.)

is nonzero,  $\alpha_s$  is so much larger than  $\beta_s$  that we can ignore the term involving  $\beta_s$  in equation 5.27. Integrating equation 5.27 under this assumption, we find that

$$P_s(t) = 1 + (P_s(0) - 1) \exp(-\alpha_s t) \quad \text{for } 0 \leq t \leq T. \quad (5.28)$$

The open probability takes its maximum value at time  $t = T$  and then, for  $t \geq T$ , decays exponentially at a rate determined by the constant  $\beta_s$ ,

$$P_s(t) = P_s(T) \exp(-\beta_s(t - T)) \quad \text{for } t \geq T. \quad (5.29)$$

If  $P_s(0) = 0$ , as it will if there is no synaptic release immediately before the release at  $t = 0$ , equation 5.28 simplifies to  $P_s(t) = 1 - \exp(-\alpha_s t)$  for  $0 \leq t \leq T$ , and this reaches a maximum value  $P_{\max} = P_s(T) = 1 - \exp(-\alpha_s T)$ . In terms of this parameter, a simple manipulation of equation 5.28 shows that we can write, in the general case,

$$P_s(T) = P_s(0) + P_{\max}(1 - P_s(0)). \quad (5.30)$$

Figure 5.14 shows a fit to a recorded postsynaptic current using this formalism. In this case,  $\beta_s$  was set to  $0.19 \text{ ms}^{-1}$ . The transmitter concentration was modeled as a square pulse of duration  $T = 1 \text{ ms}$  during which  $\alpha_s = 0.93 \text{ ms}^{-1}$ . Inverting these values, we find that the time constant determining the rapid rise seen in figure 5.14A is  $0.9 \text{ ms}$ , while the fall of the current is an exponential with a time constant of  $5.26 \text{ ms}$ .

For a fast synapse like the one shown in figure 5.14, the rise of the conductance following a presynaptic action potential is so rapid that it can be approximated as instantaneous. In this case, the synaptic conductance due to a single presynaptic action potential occurring at  $t = 0$  is often written as an exponential,  $P_s = P_{\max} \exp(-t/\tau_s)$  (see the AMPA trace in figure 5.15A), where from equation 5.29,  $\tau_s = 1/\beta_s$ . The synaptic conductance due to a

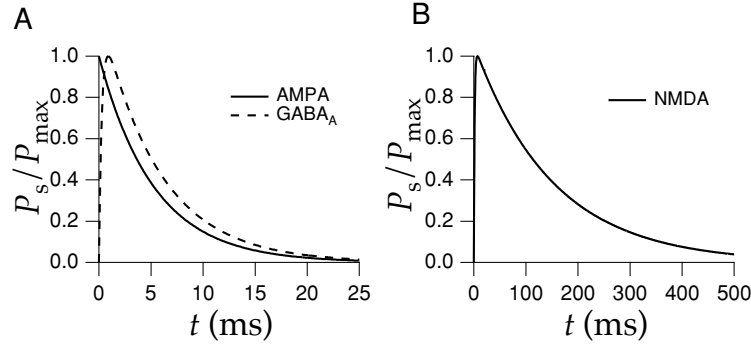


Figure 5.15 Time-dependent open probabilities fitted to match AMPA, GABA<sub>A</sub>, and NMDA synaptic conductances. (A) The AMPA curve is a single exponential described by equation 5.31 with  $\tau_s = 5.26$  ms. The GABA<sub>A</sub> curve is a difference of exponentials with  $\tau_1 = 5.6$  ms and  $\tau_{\text{rise}} = 0.3$  ms. (B) The NMDA curve is the differences of two exponentials with  $\tau_1 = 152$  ms and  $\tau_{\text{rise}} = 1.5$  ms. (Parameters are from Destexhe et al., 1994.)

sequence of action potentials at arbitrary times can be modeled by allowing  $P_s$  to decay exponentially to 0 according to the equation

$$\tau_s \frac{dP_s}{dt} = -P_s, \quad (5.31)$$

and, on the basis of the equation 5.30, making the replacement

$$P_s \rightarrow P_s + P_{\max}(1 - P_s) \quad (5.32)$$

immediately after each presynaptic action potential.

Equations 5.28 and 5.29 can also be used to model synapses with slower rise times, but other functional forms are often used. One way of describing both the rise and the fall of a synaptic conductance is to express  $P_s$  as the difference of two exponentials (see the GABA<sub>A</sub> and NMDA traces in figure 5.15). For an isolated presynaptic action potential occurring at  $t = 0$ , the synaptic conductance is written as

$$P_s = P_{\max} B (\exp(-t/\tau_1) - \exp(-t/\tau_2)), \quad (5.33)$$

where  $\tau_1 > \tau_2$ , and  $B$  is a normalization factor that assures that the peak value of  $P_s$  is equal to  $P_{\max}$ ,

$$B = \left( \left( \frac{\tau_2}{\tau_1} \right)^{\tau_{\text{rise}}/\tau_1} - \left( \frac{\tau_2}{\tau_1} \right)^{\tau_{\text{rise}}/\tau_2} \right)^{-1}. \quad (5.34)$$

The rise time of the synapse is determined by  $\tau_{\text{rise}} = \tau_1 \tau_2 / (\tau_1 - \tau_2)$ , while the fall time is set by  $\tau_1$ . This conductance reaches its peak value  $\tau_{\text{rise}} \ln(\tau_1/\tau_2)$  after the presynaptic action potential.

Another way of describing a synaptic conductance is to use the expression

$$P_s = \frac{P_{\max} t}{\tau_s} \exp(1 - t/\tau_s) \quad (5.35)$$

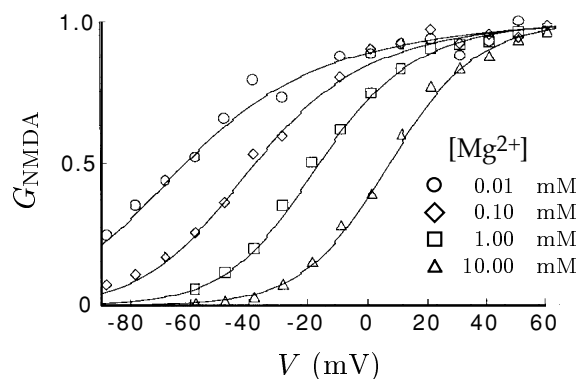


Figure 5.16 Dependence of the NMDA conductance on the membrane potential and extracellular  $\text{Mg}^{2+}$  concentration. Normal extracellular  $\text{Mg}^{2+}$  concentrations are in the range of 1 to 2 mM. The solid lines are the factors  $G_{\text{NMDA}}$  of equation 5.36 for different values of  $[\text{Mg}^{2+}]$ , and the symbols indicate the data points. (Adapted from Jahr and Stevens, 1990.)

for an isolated presynaptic release that occurs at time  $t = 0$ . This expression, called an alpha function, starts at 0, reaches its peak value at  $t = \tau_s$ , and then decays with a time constant  $\tau_s$ .

*alpha function*

We mentioned earlier in this chapter that NMDA receptor conductance has an additional dependence on the postsynaptic potential not normally seen in other conductances. To incorporate this dependence, the current due to the NMDA receptor can be described using an additional factor that depends on the postsynaptic potential,  $V$ . The NMDA current is written as  $\bar{g}_{\text{NMDA}} G_{\text{NMDA}}(V)P(V - E_{\text{NMDA}})$ .  $P$  is the usual open probability factor. The factor  $G_{\text{NMDA}}(V)$  describes an extra voltage dependence due to the fact that when the postsynaptic neuron is near its resting potential, NMDA receptors are blocked by  $\text{Mg}^{2+}$  ions. To activate the conductance, the postsynaptic neuron must be depolarized to knock out the blocking ions. Jahr and Stevens (1990) have fitted this dependence by (figure 5.16)

*NMDA receptor*

$$G_{\text{NMDA}} = \left( 1 + \frac{[\text{Mg}^{2+}]}{3.57 \text{ mM}} \exp(-V/16.13 \text{ mV}) \right)^{-1}. \quad (5.36)$$

NMDA receptors conduct  $\text{Ca}^{2+}$  ions as well as monovalent cations. Entry of  $\text{Ca}^{2+}$  ions through NMDA receptors is a critical event for long-term modification of synaptic strength. The fact that the opening of NMDA channels requires both pre- and postsynaptic depolarization means NMDA receptors can act as coincidence detectors of simultaneous pre- and postsynaptic activity. This plays an important role in connection with the Hebb rule for synaptic modification discussed in chapter 8.

*coincidence detection*



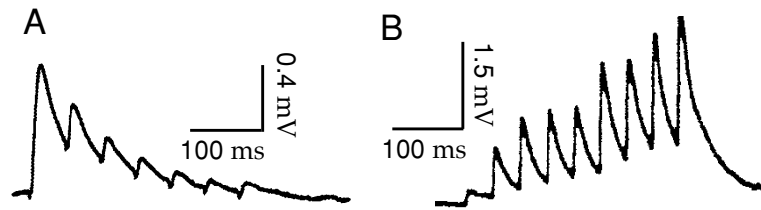


Figure 5.17 Depression and facilitation of excitatory intracortical synapses. (A) Depression of an excitatory synapse between two layer 5 pyramidal cells recorded in a slice of rat somatosensory cortex. Spikes were evoked by current injection into the presynaptic neuron, and postsynaptic potentials were recorded with a second electrode. (B) Facilitation of an excitatory synapse from a pyramidal neuron to an inhibitory interneuron in layer 2/3 of rat somatosensory cortex. (A from Markram and Tsodyks, 1996; B from Markram et al., 1998.)

## Release Probability and Short-Term Plasticity

*short-term  
plasticity*

*long-term  
plasticity*

The probability of transmitter release and the magnitude of the resulting conductance change in the postsynaptic neuron can depend on the history of activity at a synapse. The effects of activity on synaptic conductances are termed short- and long-term. Short-term plasticity refers to a number of phenomena that affect the probability that a presynaptic action potential opens postsynaptic channels and that last anywhere from milliseconds to tens of seconds. The effects of long-term plasticity are extremely persistent, lasting, for example, as long as the preparation being studied can be kept alive. The modeling and implications of long-term plasticity are considered in chapter 8. Here we present a simple way of describing short-term synaptic plasticity as a modification in the release probability for synaptic transmission. Short-term modifications of synaptic transmission can involve other mechanisms than merely changes in the probability of transmission, but for simplicity we absorb all these effects into a modification of the factor  $P_{\text{rel}}$  introduced previously. Thus,  $P_{\text{rel}}$  can be interpreted more generally as a presynaptic factor affecting synaptic transmission.

*depression  
facilitation*

Figure 5.17 illustrates two principal types of short-term plasticity, depression and facilitation. Figure 5.17A shows trial-averaged postsynaptic current pulses produced in one cortical pyramidal neuron by evoking a regular series of action potentials in a second pyramidal neuron presynaptic to the first. The pulses dramatically decrease in amplitude upon repeated activation of the synaptic conductance, revealing short-term synaptic depression. Figure 5.17B shows a similar series of averaged postsynaptic current pulses recorded in a cortical inhibitory interneuron when a sequence of action potentials was evoked in a presynaptic pyramidal cell. In this case, the amplitude of the pulses increases, and thus the synapse facilitates. In general, synapses can exhibit facilitation and depression over a variety of time scales, and multiple components of short-term plasticity can be found at the same synapse. To keep the discussion simple, we consider synapses that exhibit either facilitation or depression described by a single time constant.

Facilitation and depression can both be modeled as presynaptic processes that modify the probability of transmitter release. We describe them using a simple nonmechanistic model that has similarities to the model of  $P_s$  presented in the previous subsection. For both facilitation and depression, the release probability after a long period of presynaptic silence is  $P_{\text{rel}} = P_0$ . Activity at the synapse causes  $P_{\text{rel}}$  to increase in the case of facilitation and to decrease for depression. Between presynaptic action potentials, the release probability decays exponentially back to its “resting” value,  $P_0$ ,

$$\tau_P \frac{dP_{\text{rel}}}{dt} = P_0 - P_{\text{rel}}. \quad (5.37)$$

The parameter  $\tau_P$  controls the rate at which the release probability decays to  $P_0$ .

The models of facilitation and depression differ in how the release probability is changed by presynaptic activity. In the case of facilitation,  $P_{\text{rel}}$  is augmented by making the replacement  $P_{\text{rel}} \rightarrow P_{\text{rel}} + f_F(1 - P_{\text{rel}})$  immediately after a presynaptic action potential (as in equation 5.32). The parameter  $f_F$  (with  $0 \leq f_F \leq 1$ ) controls the degree of facilitation, and the factor  $(1 - P_{\text{rel}})$  prevents the release probability from growing larger than 1. To model depression, the release probability is reduced after a presynaptic action potential by making the replacement  $P_{\text{rel}} \rightarrow f_D P_{\text{rel}}$ . In this case, the parameter  $f_D$  (with  $0 \leq f_D \leq 1$ ) controls the amount of depression, and the factor  $P_{\text{rel}}$  prevents the release probability from becoming negative.

We begin by analyzing the effects of facilitation on synaptic transmission for a presynaptic spike train with Poisson statistics. In particular, we compute the average steady-state release probability, denoted by  $\langle P_{\text{rel}} \rangle$ .  $\langle P_{\text{rel}} \rangle$  is determined by requiring that the facilitation that occurs after each presynaptic action potential is exactly canceled by the average exponential decrement that occurs between presynaptic spikes. Consider two presynaptic action potentials separated by an interval  $\tau$ , and suppose that the release probability takes its average value  $\langle P_{\text{rel}} \rangle$  at the time of the first spike. Immediately after this spike, it is augmented to  $\langle P_{\text{rel}} \rangle + f_F(1 - \langle P_{\text{rel}} \rangle)$ . By the time of the second spike, this will have decayed to  $P_0 + (\langle P_{\text{rel}} \rangle + f_F(1 - \langle P_{\text{rel}} \rangle) - P_0) \exp(-\tau/\tau_P)$ , which is obtained by integrating equation 5.37. The average value of the exponential decay factor in this expression is the integral over all positive  $\tau$  values of  $\exp(-\tau/\tau_P)$  times the probability density for a Poisson spike train with a firing rate  $r$  to produce an interspike interval of duration  $\tau$ , which is  $r \exp(-r\tau)$  (see chapter 1). Thus, the average exponential decrement is

$$r \int_0^\infty d\tau \exp(-r\tau - \tau/\tau_P) = \frac{r\tau_P}{1 + r\tau_P}. \quad (5.38)$$

In order for the release probability to return, on average, to its steady-state value between presynaptic spikes, we must therefore require that

$$\langle P_{\text{rel}} \rangle = P_0 + (\langle P_{\text{rel}} \rangle + f_F(1 - \langle P_{\text{rel}} \rangle) - P_0) \frac{r\tau_P}{1 + r\tau_P}. \quad (5.39)$$

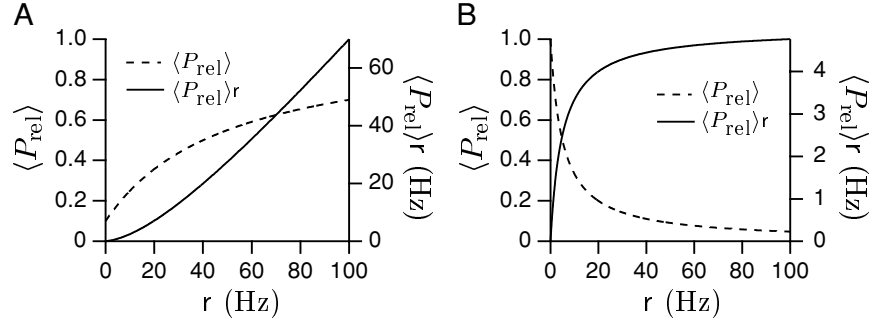


Figure 5.18 The effects of facilitation and depression on synaptic transmission. (A) Release probability and transmission rate for a facilitating synapse as a function of the firing rate of a Poisson presynaptic spike train. The dashed curve shows the rise of the average release probability as the presynaptic rate increases. The solid curve is the average rate of transmission, which is the average release probability times the presynaptic firing rate. The parameters of the model are  $P_0 = 0.1$ ,  $f_F = 0.4$ , and  $\tau_P = 50$  ms. (B) Same as A, but for the case of depression. The parameters of the model are  $P_0 = 1$ ,  $f_D = 0.4$ , and  $\tau_P = 500$  ms.

Solving for  $\langle P_{\text{rel}} \rangle$  gives

$$\langle P_{\text{rel}} \rangle = \frac{P_0 + f_F r \tau_P}{1 + r f_F \tau_P}. \quad (5.40)$$

This equals  $P_0$  at low rates and rises toward the value 1 at high rates (figure 5.18A). As a result, isolated spikes in low-frequency trains are transmitted with lower probability than spikes occurring within high-frequency bursts. The synaptic transmission rate when the presynaptic neuron is firing at rate  $r$  is the firing rate times the release probability. This is approximately  $P_0 r$  for small rates and approaches  $r$  at high rates (figure 5.18A).

The value of  $\langle P_{\text{rel}} \rangle$  for a Poisson presynaptic spike train can also be computed in the case of depression. The only difference from the above derivation is that following a presynaptic spike,  $\langle P_{\text{rel}} \rangle$  is decreased to  $f_D \langle P_{\text{rel}} \rangle$ . Thus, the consistency condition 5.39 is replaced by

$$\langle P_{\text{rel}} \rangle = P_0 + (f_D \langle P_{\text{rel}} \rangle - P_0) \frac{r \tau_P}{1 + r \tau_P}, \quad (5.41)$$

giving

$$\langle P_{\text{rel}} \rangle = \frac{P_0}{1 + (1 - f_D) r \tau_P}. \quad (5.42)$$

This equals  $P_0$  at low rates and decreases as  $1/r$  at high rates (figure 5.18B), which has some interesting consequences. As noted above, the average rate of successful synaptic transmissions is equal to  $\langle P_{\text{rel}} \rangle$  times the presynaptic rate  $r$ . Because  $\langle P_{\text{rel}} \rangle$  is proportional to  $1/r$  at high rates, the average transmission rate is independent of  $r$  in this range. This can be seen by the flattening of the solid curve in figure 5.18B. As a result, synapses

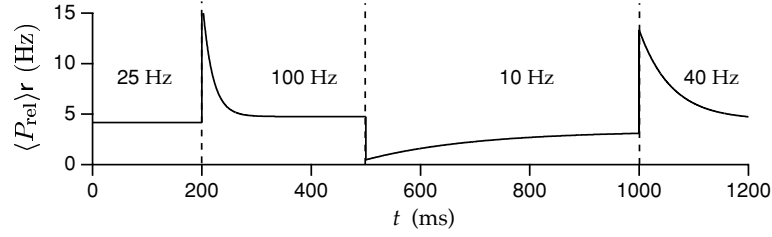


Figure 5.19 The average rate of transmission for a synapse with depression when the presynaptic firing rate changes in a sequence of steps. The firing rates were held constant at the values 25, 100, 10, and 40 Hz, except for abrupt changes at the times indicated by the dashed lines. The parameters of the model are  $P_0 = 1$ ,  $f_D = 0.6$ , and  $\tau_P = 500$  ms.

that depress do not convey information about the values of constant, high presynaptic firing rates to their postsynaptic targets. The presynaptic firing rate at which transmission starts to become independent of  $r$  is around  $1/((1 - f_D)\tau_P)$ .

Figure 5.19 shows the average transmission rate,  $\langle P_{\text{rel}} \rangle r$ , in response to a series of steps in the presynaptic firing rate. Note first that the steady-state transmission rates during the 25, 100, 10, and 40 Hz periods are quite similar. This is a consequence of the  $1/r$  dependence of the average release probability, as discussed above. The largest transmission rates in the figure occur during the sharp upward transitions between different presynaptic rates. This illustrates the important point that depressing synapses amplify transient signals relative to steady-state inputs. The transients corresponding the 25 to 100 Hz transition and the 10 to 40 Hz transition are of roughly equal amplitudes, but the transient for the 10 to 40 Hz transition is broader than that for the 25 to 100 Hz transition.

The equality of amplitudes of the two upward transients in figure 5.19 is a consequence of the  $1/r$  behavior of  $\langle P_{\text{rel}} \rangle$ . Suppose that the presynaptic firing rate makes a sudden transition from a steady value  $r$  to a new value  $r + \Delta r$ . Before the transition, the average release probability is given by equation 5.42. Immediately after the transition, before the release probability has had time to adjust to the new input rate, the average transmission rate will be this previous value of  $\langle P_{\text{rel}} \rangle$  times the new rate  $r + \Delta r$ , which is  $P_0(r + \Delta r)/(1 + (1 - f_D)r\tau_P)$ . For sufficiently high rates, this is approximately proportional to  $(r + \Delta r)/r$ . The size of the change in the transmission rate is thus proportional to  $\Delta r/r$ , which means that depressing synapses not only amplify transient inputs, they transmit them in a scaled manner. The amplitude of the transient transmission rate is proportional to the fractional change, not the absolute change, in the presynaptic firing rate. The two transients seen in figure 5.19 have similar amplitudes because in both cases  $\Delta r/r = 3$ . The difference in the recovery time for the two upward transients in figure 5.19 is due to the fact that the effective time constant governing the recovery to a new steady-state level  $r$  is  $\tau_P/(1 + (1 - f_D)r\tau_P)$ .

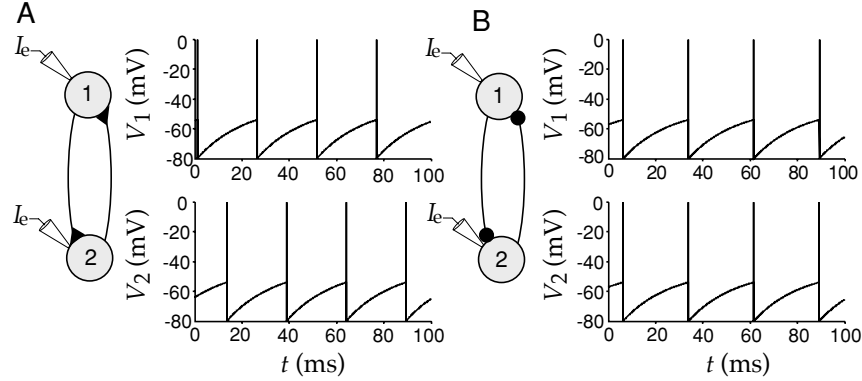


Figure 5.20 Two synaptically coupled integrate-and-fire neurons. (A) Excitatory synapses ( $E_s = 0$  mV) produce an alternating, out-of-phase pattern of firing. (B) Inhibitory synapses ( $E_s = -80$  mV) produce synchronous firing. Both model neurons have  $E_L = -70$  mV,  $V_{th} = -54$  mV,  $V_{reset} = -80$  mV,  $\tau_m = 20$  ms,  $r_m \bar{g}_s = 0.05$ ,  $P_{max} = 1$ ,  $R_m I_e = 25$  mV, and  $\tau_s = 10$  ms.

## 5.9 Synapses on Integrate-and-Fire Neurons

Synaptic inputs can be incorporated into an integrate-and-fire model by including synaptic conductances in the membrane current appearing in equation 5.8,

$$\tau_m \frac{dV}{dt} = E_L - V - r_m \bar{g}_s P_s (V - E_s) + R_m I_e. \quad (5.43)$$

For simplicity, we assume that  $P_{rel} = 1$  in this example. The synaptic current is multiplied by  $r_m$  in equation 5.43 because equation 5.8 was multiplied by this factor. To model synaptic transmission,  $P_s$  changes whenever the presynaptic neuron fires an action potential using one of the schemes described previously.

Figures 5.20A and 5.20B show examples of two integrate-and-fire neurons driven by electrode currents and connected by identical excitatory or inhibitory synapses. The synaptic conductances in this example are described by the  $\alpha$  function model. This means that the synaptic conductance a time  $t$  after the occurrence of a presynaptic action potential is given by equation 5.35. The figure shows a nonintuitive effect. When the synaptic time constant is sufficiently long ( $\tau_s = 10$  ms in this example), excitatory connections produce a state in which the two neurons fire alternately, out of phase with one another, while inhibitory synapses produce synchronous firing. It is normally assumed that excitation produces synchrony. Actually, in some cases inhibitory connections can be more effective than excitatory connections at synchronizing neuronal firing.

Synapses have multiple effects on their postsynaptic targets. In equation 5.43, the term  $r_m \bar{g}_s P_s E_s$  acts as a source of current to the neuron, while

*synchronous and  
asynchronous  
firing*

the term  $r_m \bar{g}_s P_s V$  changes the membrane conductance. The effects of the latter term are referred to as shunting, and they can be identified most easily if we divide equation 5.43 by  $1 + r_m \bar{g}_s P_s$  to obtain

$$\frac{\tau_m}{1 + r_m \bar{g}_s P_s} \frac{dV}{dt} = -V + \frac{E_L + r_m \bar{g}_s P_s E_s + R_m I_e}{1 + r_m \bar{g}_s P_s}. \quad (5.44)$$

The shunting effects of the synapse are seen in this equation as a decrease in the effective membrane time constant, and a divisive reduction in the impact of the leakage and synaptic reversal potentials and of the electrode current.

The shunting effects seen in equation 5.44 have been proposed as a possible basis for neural computations involving division. However, shunting has a divisive effect only on the membrane potential of an integrate-and-fire neuron; its effect on the firing rate is subtractive. To see this, assume that synaptic input is arriving at a sufficient rate to maintain a relatively constant value of  $P_s$ . In this case, shunting amounts to changing the value of the membrane resistance from  $R_m$  to  $R_m/(1 + r_m \bar{g}_s P_s)$ . Recalling equation 5.12 for the firing rate of the integrate-and-fire model, and the fact that  $\tau_m = C_m R_m$ , we can write the firing rate in a form that reveals its dependence on  $R_m$ ,

$$r_{\text{isi}} \approx \left[ \frac{E_L - V_{\text{th}}}{C_m R_m (V_{\text{th}} - V_{\text{reset}})} + \frac{I_e}{C_m (V_{\text{th}} - V_{\text{reset}})} \right]_+. \quad (5.45)$$

Changing  $R_m$  modifies only the constant term in this equation; it has no effect on the dependence of the firing rate on  $I_e$ .

## Regular and Irregular Firing Modes

Integrate-and-fire models are useful for studying how neurons sum large numbers of synaptic inputs and how networks of neurons interact. One issue that has received considerable attention is the degree of variability in the firing output of integrate-and-fire neurons receiving synaptic input. This work has led to the realization that neurons can respond to multiple synaptic inputs in two different modes of operation depending on the balance that exists between excitatory and inhibitory contributions.

The two modes of operation are illustrated in figure 5.21, which shows membrane potentials of an integrate-and-fire model neuron responding to 1000 excitatory and 200 inhibitory inputs. Each input consists of an independent Poisson spike train driving a synaptic conductance. The upper panels of figure 5.21 show the membrane potential with the action potential generation mechanism of the model turned off, and figures 5.21A and 5.21B illustrate the two different modes of operation. In figure 5.21A, the effect of the excitatory inputs is strong enough, relative to that of the inhibitory inputs, to make the average membrane potential, when action

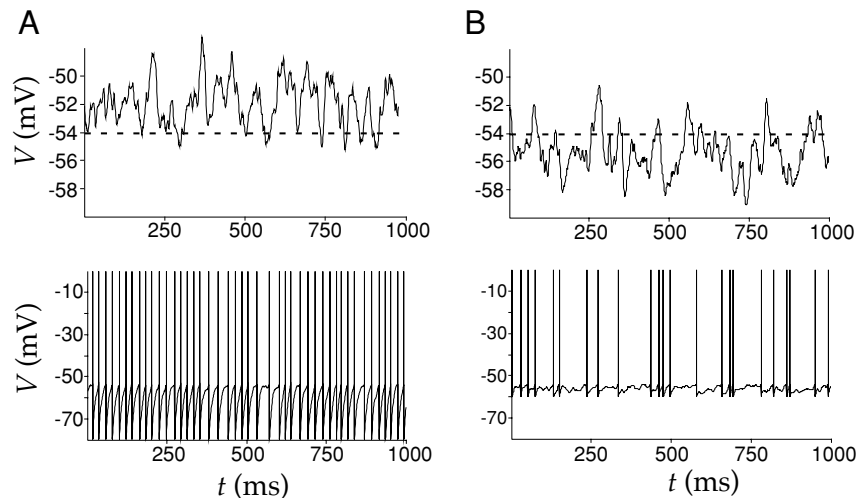


Figure 5.21 The regular and irregular firing modes of an integrate-and-fire model neuron. (A) The regular firing mode. Upper panel: The membrane potential of the model neuron when the spike generation mechanism is turned off. The average membrane potential is above the spiking threshold (dashed line). Lower panel: When the spike generation mechanism is turned on, it produces a regular spiking pattern. (B) The irregular firing mode. Upper panel: The membrane potential of the model neuron when the spike generation mechanism is turned off. The average membrane potential is below the spiking threshold (dashed line). Lower panel: When the spike generation mechanism is turned on, it produces an irregular spiking pattern. In order to keep the firing rates from differing too greatly between these two examples, the value of the reset voltage is higher in B than in A.

potential generation is blocked, more depolarized than the spiking threshold of the model (the dashed line in the figure). When the action potential mechanism is turned on (lower panel of figure 5.21A), this produces a fairly regular pattern of action potentials.

The irregularity of a spike train can be quantified using the coefficient of variation ( $C_V$ ), the ratio of the standard deviation to the mean of the interspike intervals (see chapter 1). For the Poisson inputs being used in this example,  $C_V = 1$ , while for the spike train in the lower panel of figure 5.21A,  $C_V = 0.3$ . Thus, the output spike train is much more regular than the input trains. This is not surprising, because the model neuron effectively averages its many synaptic inputs. In the regular firing mode, the total synaptic input attempts to charge the neuron above the threshold, but every time the potential reaches the threshold, it gets reset and starts charging again. In this mode of operation, the timing of the action potentials is determined primarily by the charging rate of the cell, which is controlled by its membrane time constant.

Figure 5.21B shows the other mode of operation that produces an irregular firing pattern. In the irregular firing mode, the average membrane potential is more hyperpolarized than the threshold for action potential generation (upper panel of figure 5.21B). Action potentials are generated

only when there is a fluctuation in the total synaptic input strong enough to make the membrane potential reach the threshold. This produces an irregular spike train, such as that seen in the lower panel of figure 5.21B, which has a  $C_V$  value of 0.84.

The high degree of variability seen in the spiking patterns of in vivo recordings of cortical neurons (see chapter 1) suggests that they are better approximated by an integrate-and-fire model operating in an irregular-firing mode. There are advantages to operating in the irregular-firing mode that may compensate for its increased variability. One is that neurons firing in the irregular mode reflect in their outputs the temporal properties of fluctuations in their total synaptic input. In the regular firing mode, the timing of output spikes is only weakly related to the temporal character of the input spike trains. In addition, neurons operating in the irregular firing mode can respond more quickly to changes in presynaptic spiking patterns and firing rates than those operating in the regular firing mode.

## 5.10 Chapter Summary

In this chapter, we considered the basic electrical properties of neurons, including their intracellular and membrane resistances, capacitances, and active voltage-dependent and synaptic conductances. We introduced the Nernst equation for equilibrium potentials and the formalism of Hodgkin and Huxley for describing persistent, transient, and hyperpolarization-activated conductances. Methods were introduced for modeling stochastic channel opening and stochastic synaptic transmission, including the effects of synaptic facilitation and depression. We discussed a number of ways of describing synaptic conductances following the release of a neurotransmitter. Two models of action potential generation were discussed, the simple integrate-and-fire scheme and the more realistic Hodgkin-Huxley model.

## 5.11 Appendices

### A: Integrating the Membrane Potential

We begin by considering the numerical integration of equation 5.8. It is convenient to rewrite this equation in the form

$$\tau_V \frac{dV}{dt} = V_\infty - V, \quad (5.46)$$

where  $\tau_V = \tau_m$  and  $V_\infty = E_L + R_m I_e$ . When the electrode current  $I_e$  is independent of time, the solution of this equation is

$$V(t) = V_\infty + (V(t_0) - V_\infty) \exp(-(t - t_0)/\tau_V), \quad (5.47)$$



where  $t_0$  is any time prior to  $t$  and  $V(t_0)$  is the value of  $V$  at time  $t_0$ . Equation 5.9 is a special case of this result with  $t_0 = 0$ .

If  $I_e$  depends on time, the solution 5.47 is not valid. An analytic solution can still be written down in this case, but it is not particularly useful except in special cases. Over a small enough time period  $\Delta t$ , we can approximate  $I_e(t)$  as constant and use the solution 5.47 to step from a time  $t$  to  $t + \Delta t$ . This requires replacing the variable  $t_0$  in equation 5.47 with  $t$ , and  $t$  with  $t + \Delta t$ , so that

$$V(t + \Delta t) = V_\infty + (V(t) - V_\infty) \exp(-\Delta t / \tau_V). \quad (5.48)$$

This equation provides an updating rule for the numerical integration of equation 5.46. Provided that  $\Delta t$  is sufficiently small, repeated application of the update rule 5.48 provides an accurate way of determining the membrane potential. Furthermore, this method is stable because if  $\Delta t$  is too large, it will only move  $V$  toward  $V_\infty$  and not, for example, make it grow without bound.

The equation for a general single-compartment conductance-based model, equation 5.6 with 5.5, can be written in the same form as equation 5.46 with

$$V_\infty = \frac{\sum_i g_i E_i + I_e / A}{\sum_i g_i} \quad (5.49)$$

and

$$\tau_V = \frac{c_m}{\sum_i g_i}. \quad (5.50)$$

Note that if  $c_m$  is in units of nF/mm<sup>2</sup> and the conductances are in the units  $\mu S/mm^2$ ,  $\tau_V$  comes out in ms units. Similarly, if the reversal potentials are given in units of mV,  $I_e$  is in nA, and  $A$  is in mm<sup>2</sup>,  $V_\infty$  will be in mV units.

If we take the time interval  $\Delta t$  to be small enough so that the gating variables can be approximated as constant during this period, the membrane potential can again be integrated over one time step, using equation 5.48. Of course, the gating variables are not fixed, so once  $V$  has been updated by this rule, the gating variables must be updated as well.

## B: Integrating the Gating Variables

All the gating variables in a conductance-based model satisfy equations of the same form,

$$\tau_z \frac{dz}{dt} = z_\infty - z, \quad (5.51)$$

where we use  $z$  to denote a generic variable. Note that this equation has the same form as equation 5.46, and it can be integrated in exactly the same way. We assume that  $\Delta t$  is sufficiently small so that  $V$  does not change appreciably over this time interval (and similarly  $[Ca^{2+}]$  is approximated as

constant over this interval if any of the conductances are  $\text{Ca}^{2+}$ -dependent). Then,  $\tau_z$  and  $z_\infty$ , which are functions of  $V$  (and possibly  $[\text{Ca}^{2+}]$ ) can be treated as constants over this period and  $z$  can be updated by a rule identical to 5.48,

$$z(t + \Delta t) = z_\infty + (z(t) - z_\infty) \exp(-\Delta t / \tau_z). \quad (5.52)$$

An efficient integration scheme for conductance-based models is to alternate using rule (5.48) to update the membrane potential and rule (5.52) to update all the gating variables. It is important to alternate the updating of  $V$  with that of the gating variables, rather than doing them all simultaneously, as this keeps the method accurate to second order in  $\Delta t$ . If  $\text{Ca}^{2+}$ -dependent conductances are included, the intracellular  $\text{Ca}^{2+}$  concentration should be computed simultaneously with the membrane potential. By alternating the updating, we mean that the membrane potential is computed at times  $0, \Delta t, 2\Delta t, \dots$ , while the gating variables are computed at times  $\Delta t/2, 3\Delta t/2, 5\Delta t/2, \dots$ . A discussion of the second-order accuracy of this scheme is given in Mascagni and Sherman (1998).

## 5.12 Annotated Bibliography

**Jack et al. (1975)**, **Tuckwell (1988)**, **Johnston & Wu (1995)**, **Koch & Segev (1998)**, and **Koch (1998)** cover much of the material in this chapter and in chapter 6. **Hille (1992)** provides a comprehensive treatment of ion channels. **Hodgkin & Huxley (1952)** presents the classic biophysical model of the action potential, and **Sakmann & Neher (1983)** describes patch clamp recording techniques allowing single channels to be studied electrophysiologically.

The integrate-and-fire model was introduced by Lapicque (1907). **Destexhe et al. (1994)** describes kinetic models of both ion channels and short-term postsynaptic effects at synapses. Marom & Abbott (1994) shows how the  $\text{Na}^+$  channel model of Patlak (1991) can be reconciled with typical macroscopic conductance models. For a review of the spike-response model, the integrated version of the integrate-and-fire model, see **Gerstner (1998)**. Wang (1994) analyzes a spike-rate adaptation model similar to the one we presented, and Stevens & Zador (1998) introduces an integrate-and-fire model with time-dependent parameters.

The dynamic aspects of synaptic transmission are reviewed in **Magleby (1987)** and **Zucker (1989)**. Our presentation followed Abbott et al. (1997), Varela et al. (1997), and Tsodyks & Markram (1997). For additional implications of short-term synaptic plasticity for cortical processing, see Lisman (1997) and Chance et al. (1998). Wang & Rinzel (1992) notes that inhibitory synapses can synchronize coupled cells, and in our discussion we followed the treatment in van Vreeswijk et al. (1994). Our analysis of the regular and irregular firing mode regimes of integrate-and-fire cells was

based on Troyer & Miller (1997). Numerical methods for integrating the equations of neuron models are discussed in **Mascagni & Sherman (1998)**.

This excerpt from  
Theoretical Neuroscience  
Computational and Mathematical Modeling of Neural Systems  
Peter Dayan and L. F. Abbott  
© 2001 The MIT Press.

is provided in screen-viewable form for personal use only by members  
of MIT CogNet.

Unauthorized use or dissemination of this information is expressly  
forbidden.

If you have any questions about this material, please contact  
[cognetadmin@cognet.mit.edu](mailto:cognetadmin@cognet.mit.edu).